

# The fate of small classically stable $Q$ -balls

---

Dmitry Levkov<sup>a,b</sup> Emin Nugaev<sup>a,b</sup> Andrei Popescu<sup>a,c,d</sup>

<sup>a</sup>*Institute for Nuclear Research of the Russian Academy of Sciences, 60th October Anniversary Prospect 7a, Moscow 117312, Russia*

<sup>b</sup>*Moscow Institute of Physics and Technology, Institutskii per. 9, Dolgoprudny 141700, Moscow Region, Russia*

<sup>c</sup>*Faculty of Physics, Moscow State University, Moscow 119991, Russia*

<sup>d</sup>*Department of Applied Mathematics and Theoretical Physics, University of Cambridge, Wilberforce Road, Cambridge CB3 0WA, UK*

*E-mail:* [levkov@ms2.inr.ac.ru](mailto:levkov@ms2.inr.ac.ru), [emin@ms2.inr.ac.ru](mailto:emin@ms2.inr.ac.ru),  
[popescu@ms2.inr.ac.ru](mailto:popescu@ms2.inr.ac.ru)

**ABSTRACT:** The smallest classically stable  $Q$ -balls are, in fact, generically metastable: in quantum theory they decay into free particles via collective tunneling. We derive general semiclassical method to calculate the rate of this process in the entire kinematical region of  $Q$ -ball metastability. Our method uses Euclidean field-theoretical solutions resembling the Coleman's bounce and fluctuations around them. As an application of the method, we numerically compute the decay rate to the leading semiclassical order in a particular one-field model. We shortly discuss cosmological implications of metastable  $Q$ -balls.

---

## Contents

|          |   |           |
|----------|---|-----------|
| <b>1</b> | <b>Introduction</b>                             | <b>1</b>  |
| <b>2</b> | <b>Semiclassical method and its application</b> | <b>5</b>  |
| 2.1      | Metastable $Q$ -balls                           | 5         |
| 2.2      | Euclidean solutions for the decay probability   | 7         |
| 2.3      | Applying the method                             | 10        |
| 2.4      | Decay at finite temperature                     | 12        |
| <b>3</b> | <b>Derivation of the semiclassical method</b>   | <b>13</b> |
| 3.1      | Quantum states for $Q$ -balls                   | 13        |
| 3.2      | Decay probability in the form of path integral  | 14        |
| 3.3      | Saddle-point approximation                      | 16        |
| 3.4      | Expression for the prefactor                    | 18        |
| 3.5      | Finite-temperature solutions                    | 20        |
| <b>4</b> | <b>Numerical implementation</b>                 | <b>20</b> |
| 4.1      | Framework                                       | 20        |
| 4.2      | Obtaining the solutions                         | 21        |
| <b>5</b> | <b>Discussion: Prospects for cosmology</b>      | <b>24</b> |
| <b>A</b> | <b>Solitons and their (in)stability</b>         | <b>27</b> |

---

## 1 Introduction

It is well-known that  $Q$ -balls [1–3], the solitonic “bags” with attractive globally charged particles inside, are rock stable if their total charges  $Q$  are large and the model has a mass gap  $m$ . Indeed, the net masses  $E_Q$  of these objects include negative energy of particle attraction and, as a consequence, grow slowly as the new particles are added,  $E_Q \propto Q^a$ ,  $a < 1$  [3]. This makes sufficiently large  $Q$ -balls lighter than the sets of massive particles with the same charge,  $E_Q < mQ$ , and their fission — forbidden by energy and charge conservation.<sup>1</sup>

---

<sup>1</sup>If massless charged particles are present, the  $Q$ -balls may evaporate by emitting them from the surface [4, 5]. Below we assume that this process, if exists, occurs at negligibly small rate.

Exceptional stability singles out  $Q$ -balls as the favorite toys for cosmologists [6]. These objects may be generated in the early Universe via first-order phase transition [7–9] or fragmentation of the scalar condensate [10–12] to form dark matter at the present epoch. They may also participate in the Affleck-Dine baryogenesis [13–15] catalyzing the process and hiding the baryon number from the sphaleron transitions [16, 17]. In the recklessly exotic scenario  $Q$ -balls may even impersonate black holes [18] posing new challenges for the astrophysical observations [19, 20]. As a pleasant bonus, the objects of this kind invariably appear [21] in supersymmetric models with flat directions which remain in the club of our favorite extensions of the Standard Model despite obvious lack of support from the experimental data [22].

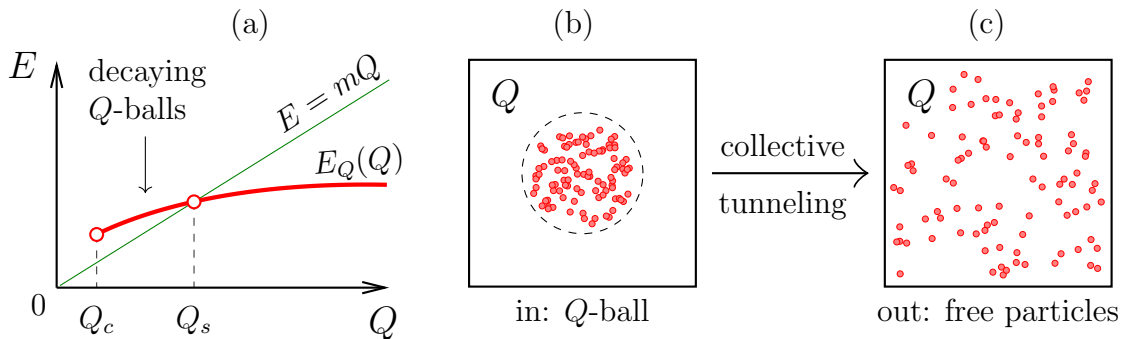


**Figure 1.** (a) Typical dependence of  $Q$ -ball mass  $E_Q$  on its charge  $Q$  (thick solid line). (b), (c) Decay of small  $Q$ -ball into free particles.

Weak dependence of  $Q$ -ball mass  $E_Q$  on its charge has another, less widely recognized consequence. At smallest  $Q$  this mass exceeds the minimal energy  $mQ$  of free particles, which makes small  $Q$ -balls generically unstable [1–3] in some region  $Q < Q_s$ ,  $E_{Q_s} = mQ_s$ , see Fig. 1a. Still, these objects are classically stable if  $Q$  is slightly below  $Q_s$ . Indeed, the energy deficit  $E_Q - mQ$  of their decay would be small, as well as the momenta of the final-state particles. But finite-size solitons like that cannot evolve classically into waves/particles of much larger wavelength! This gives a range of charges  $Q_c < Q < Q_s$  where the  $Q$ -balls exist, remain classically stable and yet, decay into free particles quantum-mechanically. Being local minima of energy at fixed charge, they cannot “leak” the particles one-by-one. Rather, they remain metastable for a long time and then explode in a spectacular collective tunneling event sketched in Fig. 1b. We stress that the metastability window  $Q_c < Q < Q_s$  of global  $Q$ -balls appears in all three-dimensional models with bounded energy considered in literature, see e.g. [1, 3, 23, 24].

In this paper we develop general semiclassical method to compute the decay rate of metastable  $Q$ -balls at  $Q, Q_c, Q_s \gg 1$ . To the best of our knowledge, no method of

this kind has been ever proposed before, with the closest example describing quantum collapse of a metastable Bose condensate in condensed matter physics [25]. There are two reasons, why. First, the states of  $Q$ -balls are not just the local minima of energy like the false vacua [26], but the minima at a fixed charge  $Q$ . Second, the charged scalar particles inside the  $Q$ -ball are typically described by an oscillating complex scalar field  $\varphi(\mathbf{x}, t) \propto e^{i\omega t}$  which grows without bound in Euclidean time  $\tau \equiv it$ . These features do not enable one to use powerful techniques developed for false vacuum decay [27–29], or even perform Wick rotation at the start of calculations.

Our semiclassical method is derived by evaluating path integral for the  $Q$ -ball decay rate in the saddle-point approximation [30–34] and going into Euclidean time afterwards. This general procedure is justified at  $Q \gg 1$ . We arrive at the semiclassical expression for the rate in terms of a certain classical solution  $\varphi = \varphi_{cl}(\mathbf{x}, \tau)$  which resembles the Coleman’s bounce [27] in Euclidean time  $\tau$  and yet, differs from it in important details. Our solution interpolates between the  $Q$ -ball at  $\tau \rightarrow -\infty$  and configuration in the catchment area of the vacuum at  $\tau = 0$ . Unlike the bounce, it can be continued to Euclidean time only in a very specific way, by turning the charged field  $\varphi$  and its complex conjugate  $\bar{\varphi}$  into independent real functions of  $\mathbf{x}$  and  $\tau$ . The real ratio  $\varphi_{cl}/\bar{\varphi}_{cl}$  satisfies certain boundary conditions at  $\tau = -\infty$  and  $\tau = 0$ . Given the solution, one computes the probability of  $Q$ -ball decay per unit time,

$$\Gamma_Q = A_Q \cdot e^{-F_Q} , \quad (1.1)$$

where the suppression exponent  $F_Q$  is related to Euclidean action on  $\varphi_{cl}$  and the prefactor  $A_Q$  includes fluctuation determinant around this solution. In the semiclassical limit  $Q \sim Q_c \gg 1$  the exponent  $F_Q \propto Q_c$  becomes large, and  $A_Q \sim mQ_c^{1/2}$ .

As a by-product, we obtain expression for the width of metastable  $Q$ -balls interacting with neutral finite-temperature bath. In this case the semiclassical solution lives on a finite Euclidean time interval and expressions for the exponent and the prefactor are modified accordingly.

We illustrate the semiclassical method in the model of a complex scalar field  $\varphi(\mathbf{x}, t)$ ,

$$S = \int d^3\mathbf{x} dt [\partial_\mu \varphi \partial^\mu \bar{\varphi} - V(\varphi \bar{\varphi})] , \quad (1.2)$$

with scalar potential shown in Fig. 2a. Overbar in Eq. (1.2) and below denotes complex conjugation, expression for  $V(\varphi \bar{\varphi})$  will be given in the main text. Note that our model approximates renormalizable Friedberg-Lee-Sirlin two-field model [1] in the limit when the additional field is very massive and can be integrated out. Besides, the potential in Fig. 2a is flat at large fields:  $V \approx \Lambda^4$  at  $|\varphi| > v$ . In this regard it is similar to potentials appearing in supersymmetric theories with flat directions [21].

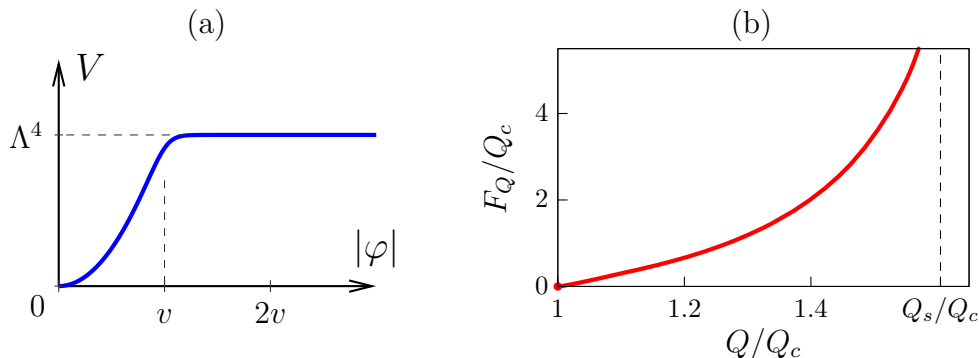


**Figure 2.** (a) Scalar potential used in the numerical calculations. (b) Suppression exponent for the rate of  $Q$ -ball decay in the model with potential (a).

The model (1.2) has a family of  $Q$ -ball solutions with mass graph  $E_Q = E_Q(Q)$  similar to the one in Fig. 1a. These objects are metastable at charges between  $Q_c \approx 266 v^4/\Lambda^4$  and  $Q_s \approx 1.6 Q_c$ . At  $v > 5\Lambda$  the values of  $Q_c$  and  $Q_s$  are large and semiclassical approximation can be used for all metastable  $Q$ -balls. We numerically found the respective semiclassical solutions  $\varphi_{cl}(\mathbf{x}, \tau)$  and computed the suppression exponent  $F_Q$  of the decay rate, see Fig. 2b. As expected, the value of  $F_Q$  tends to zero and infinity in the limits  $Q \rightarrow Q_c$  and  $Q \rightarrow Q_s$  corresponding to classically decaying and absolutely stable  $Q$ -balls. Leaving numerical calculation of the fluctuation determinant to further studies, we roughly estimate the prefactor in Eq. (1.1) as  $A_Q \sim mQ_c^{1/2} \sim 10v$ .

In cosmology metastable  $Q$ -balls may form naturally long-living decaying dark matter. In the most exciting scenario the lifetime of these objects is comparable to the age of the Universe, so that their decays can affect structure formation and alleviate [35] emerging tension between the low-redshift [36, 37] and high-redshift (CMB) [38] cosmological measurements. This requires, however, moderately small  $Q$ -ball charges  $Q \sim Q_c \sim F_Q$ : in the above model  $\Gamma_Q^{-1}$  is of order  $10^{10}$  years if  $Q \sim Q_c \sim 10^2$ , see Fig. 2b. Our estimates show that the  $Q$ -balls with these charges may be generated in the early Universe via phase transition or fragmentation of the scalar condensate if the generation temperature is raised to  $T \sim 10^{11}$  GeV, cf. [39]. Besides, alternative generation mechanisms — say, pair production [40] — may be essential at small  $Q$ . This suggests a path to new cosmological scenarios with metastable  $Q$ -balls which may be considered separately.

In the introductory Sec. 2 we explain our semiclassical method and show main numerical results. Derivation of the method and details of its numerical implementation are given in Secs. 3 and 4, respectively. We discuss possible cosmological applications of the metastable  $Q$ -balls in Sec. 5.

## 2 Semiclassical method and its application

### 2.1 Metastable $Q$ -balls

We start by briefly reviewing the properties of small  $Q$ -balls. To be concrete, consider the model (1.2) of complex scalar field  $\varphi$  with the potential

$$V = -\frac{m^2 v^2}{b} \log \left( \frac{e^{-b\varphi\bar{\varphi}/v^2} + e^{-b}}{1 + e^{-b}} \right), \quad b = 8 \quad (2.1)$$

shown in Fig. 2a. The scalar bosons in this model have mass  $\approx m$  in vacuum  $\varphi = 0$  and become almost massless at large  $\varphi$ :  $V \rightarrow \Lambda^4 \equiv m^2 v^2 \log(e^b + 1)/b$  as  $|\varphi| \rightarrow +\infty$ . This corresponds to short-range attraction between the bosons. Importantly, the potential (2.1) approximately describes decoupling limit of the renormalizable Friedberg-Lee-Sirlin model [1], as we will argue in Sec. 5.

The model (1.2) possesses global conserved charge

$$Q = i \int d^3 \mathbf{x} (\varphi \partial_t \bar{\varphi} - \bar{\varphi} \partial_t \varphi), \quad (2.2)$$

related to phase rotation symmetry  $\varphi \rightarrow e^{-i\alpha} \varphi$ ,  $\bar{\varphi} \rightarrow e^{i\alpha} \bar{\varphi}$ . Conservation of this quantity is vital [2] for the existence and stability of  $Q$ -balls — nontopological solitons carrying nonzero  $Q$ .

In what follows we use semiclassical approximation which is justified at  $g \equiv m/v \ll 1$ . Indeed, change of variables  $\varphi \rightarrow v\varphi$ ,  $x^\mu \rightarrow x^\mu/m$  eliminates all parameters from the classical action (1.2), (2.1) except for the combination  $g^{-2}$  right in front of it. This means that  $g^2 \ll 1$  is the semiclassical parameter in our model. Besides, the charge (2.2) also becomes proportional to  $g^{-2}$  after the change of variables suggesting that  $Q \gg 1$  in the semiclassical regime.

The simplest way to find nontopological solitons in the model (2.1) is to substitute stationary spherically-symmetric Ansatz

$$\varphi_Q(\mathbf{x}, t) = \chi_Q(r) e^{i\omega t}, \quad r = |\mathbf{x}|, \quad (2.3)$$

into the classical field equations and numerically solve the remaining ordinary differential equation for the real function  $\chi_Q(r)$  with regularity conditions  $\partial_r \chi_Q(0) = \chi_Q(\infty) = 0$ , see Appendix A for details. This gives a family of localized solutions parametrized with the frequency  $\omega$ , see two of them in Fig. 3a. In Fig. 3b we show the charges  $Q = Q(\omega)$  of all solutions, Eq. (2.2). Quite surprisingly, no solution exists at  $Q < Q_c \approx 266/g^2$ . At the same time, two solutions, the “ $Q$ -ball” and “ $Q$ -cloud”, are present at each  $Q > Q_c$ ; the respective subfamilies are marked by solid and thick-dashed lines in Fig. 3b.

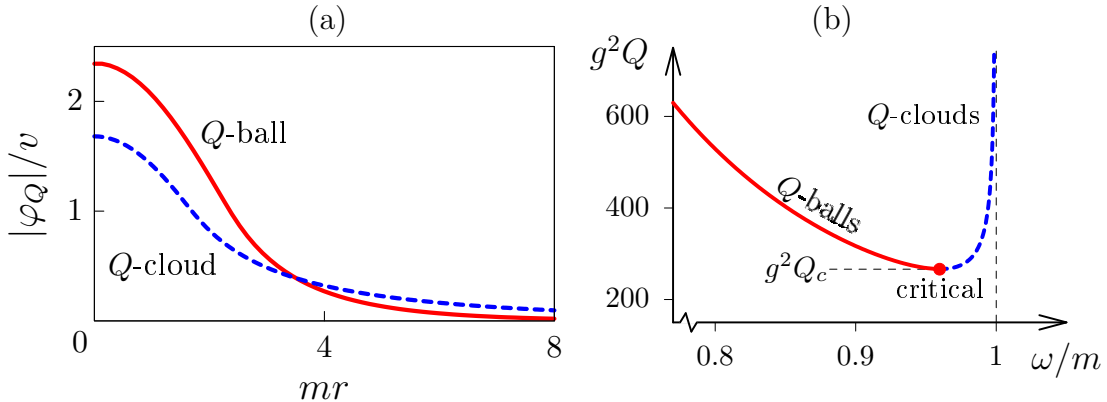


**Figure 3.** (a) Profiles  $|\varphi_Q|$  of nontopological solitons with  $\omega \approx 0.88m$  and  $0.99m$  in the model (2.1) (solid and dashed lines, respectively). The charges of these solutions are equal:  $g^2Q = 353$  ( $Q/Q_c \approx 1.33$ ). (b) Soliton charge  $Q$  as a function of its frequency  $\omega$ .

To explain these features, we recall the main property of nontopological solitons proven in [2]: stationary solutions of the form (2.3) are, in fact, extrema of energy

$$E = \int d^3\mathbf{x} [\partial_t\varphi\partial_t\bar{\varphi} + \nabla_{\mathbf{x}}\varphi\nabla_{\mathbf{x}}\bar{\varphi} + V(\varphi\bar{\varphi})] \quad (2.4)$$

in the subsector of field configurations  $\{\varphi(\mathbf{x}), \partial_t\varphi(\mathbf{x})\}_Q$  with fixed charge  $Q$ . Computing the total masses (2.4) of all solutions, we find that the  $Q$ -clouds are always heavier than the  $Q$ -balls with the same charge, see Fig. 4a. Besides, the  $Q$ -clouds are classically unstable: they do not satisfy the rigorous Vakhitov-Kolokolov criterion  $dQ/d\omega \leq 0$  [41–43] which is necessary for stability, cf. Fig. 3b. This suggests the structure of the energy functional in the subsector of configurations with fixed  $Q$  shown in Fig. 4b. The  $Q$ -ball and a configuration describing  $Q$  free particles at rest are the two local minima of  $E$  at fixed  $Q$  separated by an energy barrier. The  $Q$ -cloud, to the contrary, is an unstable stationary solution “sitting” precisely on the barrier top [44]; the analogous solutions in scalar theories with false vacuum decay and in gauge theories are called critical bubble [26, 27, 29] and sphaleron [45], respectively.

In Appendix A we confirm the picture in Fig. 4b by demonstrating that all  $Q$ -balls in our model are classically stable, while the  $Q$ -clouds have precisely one unstable mode.

In quantum theory the global minimum of energy in Fig. 4b corresponds to true ground state at a given  $Q$ , while the other, local minimum represents metastable state decaying via tunneling through the potential barrier. It is clear from Fig. 4a that the  $Q$ -balls are metastable at  $Q_c < Q < Q_s$  when their masses exceed the energies  $mQ$

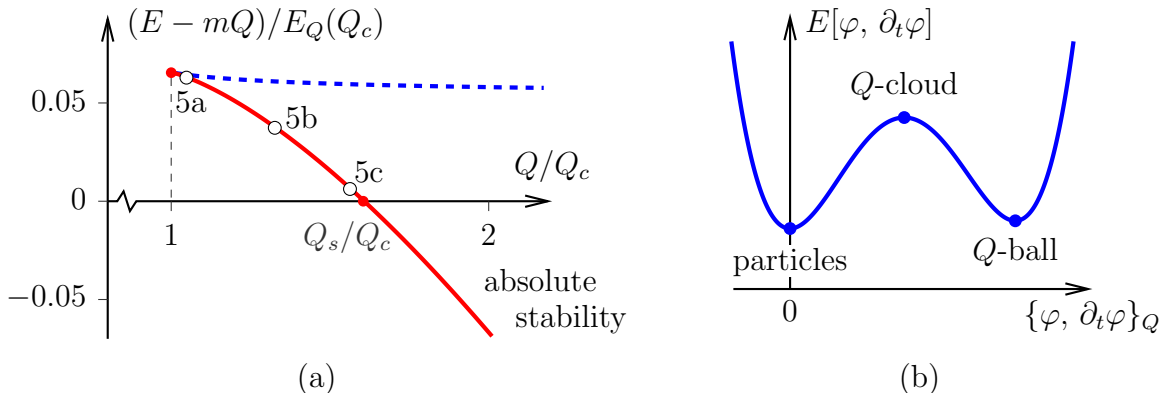


**Figure 4.** (a) Binding energies  $E - mQ$  of  $Q$ -balls and  $Q$ -clouds as functions of their charges  $Q$  (solid and dashed lines, respectively). Empty circles show parameters of the tunneling solutions in Figs. 5a-c. (b) Schematic form of the energy functional  $E[\varphi, \partial_t \varphi]$  in the subspace of configurations  $\{\varphi(\mathbf{x}), \partial_t \varphi(\mathbf{x})\}_Q$  with fixed charge  $Q$ .

of free particles with the same charge. Below we compute the lifetimes  $\Gamma_Q^{-1}$  of these objects.

Direct inspection of literature [1, 3, 23, 24, 44, 46, 47] shows that the above picture is typical in weakly interacting theories with bounded energies possessing  $Q$ -ball solutions. Namely, nontopological solitons in these models can be sorted into classically stable  $Q$ -balls — local minima of energy at fixed charge — and  $Q$ -clouds “sitting” on tops of the potential barriers between the  $Q$ -balls and free particles in the vacuum. The branches of  $Q$ -balls and  $Q$ -clouds meet at the critical point  $Q = Q_c$ ,  $E = E_Q(Q_c)$  corresponding to the smallest soliton at the verge of classical stability. By construction, the  $Q$ -cloud masses are higher than the minimal values of energy  $E_Q$  and  $mQ$ . Thus, the critical mass also satisfies  $E_Q(Q_c) > mQ$  implying that there exists a window of charges  $Q_c < Q < Q_s$  where the  $Q$ -balls are metastable,  $E_Q > mQ$ .

## 2.2 Euclidean solutions for the decay probability

Let us preview our semiclassical recipe to calculate  $\Gamma_Q$  postponing its derivation till Sec. 3. For illustrative purposes we will compare this recipe to the powerful Euclidean technique [27–29] developed for the decay of metastable (false) vacuum in models of real scalar field(s)  $\phi$  without conserved charges. The latter process is described by the “bounce” — real Euclidean solution  $\phi_{cl}(\mathbf{x}^2 + \tau^2)$  interpolating between the false vacuum at  $\tau \rightarrow -\infty$  and the catchment area of the true vacuum at  $\tau = 0$ . After continuation to Minkowski time  $t \equiv -i\tau > 0$  this solution describes classical evolution of an expanding true vacuum bubble in the final state. The rate of false vacuum decay is given by the expression similar to Eq. (1.1), where the leading suppression exponent is Euclidean



action of the bounce  $S_E[\phi_{cl}]$  and the prefactor includes fluctuation determinant around this solution.

We expect to find similar, though properly modified, procedure for computing the rate of  $Q$ -ball decay. In Sec. 3 we indeed introduce the semiclassical solution  $\varphi_{cl}(\mathbf{x}, \tau)$ ,  $\bar{\varphi}_{cl}(\mathbf{x}, \tau)$  satisfying Euclidean field equations in the model (1.2),

$$(\partial_\tau^2 + \nabla_{\mathbf{x}}^2)\varphi_{cl} = V'\varphi_{cl}, \quad (\partial_\tau^2 + \nabla_{\mathbf{x}}^2)\bar{\varphi}_{cl} = V'\bar{\varphi}_{cl}, \quad (2.5)$$

where  $V'$  is a derivative of  $V(\bar{\varphi}\varphi)$  with respect to its argument. Our solution is spherically-symmetric, i.e. depends on  $r \equiv |\mathbf{x}|$  and  $\tau$ . It is natural to expect that it coincides with the  $Q$ -ball (2.3) at the start of the process,

$$\varphi_{cl} \rightarrow e^{\omega\tau - \eta_0/2} \chi_Q(r), \quad \bar{\varphi}_{cl} \rightarrow e^{-\omega\tau + \eta_0/2} \chi_Q(r) \quad \text{as} \quad \tau \rightarrow -\infty, \quad (2.6)$$

where we introduced the time shift  $\eta_0$  that cannot be excluded in general. In Sec. 3 we obtain the boundary condition

$$\varphi_{cl} = e^{-\omega\beta - \eta_0} \bar{\varphi}_{cl}, \quad \partial_\tau \varphi_{cl} = -e^{-\omega\beta - \eta_0} \partial_\tau \bar{\varphi}_{cl} \quad \text{at} \quad \tau = -\frac{\beta}{2} \rightarrow -\infty, \quad (2.7)$$

which is consistent with the asymptotics (2.6). Soon we will verify numerically that the solutions of Eqs. (2.5), (2.7) automatically satisfy Eq. (2.6).

Surprisingly,  $\varphi_{cl}$  and  $\bar{\varphi}_{cl}$  in Eq. (2.6) are not complex conjugate to each other. This is not a problem, however, for the complex semiclassical method adopted in Sec. 3. Instead, our derivation suggests that  $\varphi_{cl}$  and  $\bar{\varphi}_{cl}$  should be considered as independent *real* functions of  $\mathbf{x}$  and  $\tau$ . Then the value of Euclidean action

$$S_E \equiv -iS = \int_{-\beta/2}^{\beta/2} d\tau d^3\mathbf{x} [\partial_\tau \varphi \partial_\tau \bar{\varphi} + \nabla_{\mathbf{x}} \varphi \nabla_{\mathbf{x}} \bar{\varphi} + V(\varphi \bar{\varphi})] \quad (2.8)$$

is real, where  $\beta$  will be sent to infinity in the end of the calculation.

Like the bounce, our semiclassical solution arrives to the catchment area of the true vacuum at  $\tau = 0$ . To quantify this criterion, we use the second boundary condition derived in Sec. 3,

$$\varphi_{cl} = \bar{\varphi}_{cl}, \quad \partial_\tau \varphi_{cl} = -\partial_\tau \bar{\varphi}_{cl} \quad \text{at} \quad \tau = 0. \quad (2.9)$$

This means that the solution is symmetric with respect to time reflections,  $\varphi_{cl}(\mathbf{x}, \tau) = \bar{\varphi}_{cl}(\mathbf{x}, -\tau)$ . As a consequence, after continuation to Minkowski time  $t = -i\tau > 0$  the functions  $\varphi_{cl}$  and  $\bar{\varphi}_{cl}$  become complex conjugate to each other, i.e. represent ordinary classical evolution after the decay. We expect to obtain free waves/particles classically evolving in the vacuum as  $t \rightarrow +\infty$ .

Solving Eqs. (2.5) with boundary conditions (2.7), (2.9) at large  $\beta$ , one finds a family of real solutions  $\varphi_{cl}, \bar{\varphi}_{cl}$  parametrized with  $\omega\beta + \eta_0$  in Eq. (2.7). Apparently, different values of this combination correspond to solutions approaching different  $Q$ -balls at large negative  $\tau$ . In what follows we express  $\eta_0 = \eta_0(Q)$  using Eq. (2.2) and characterize the solutions with charge  $Q$ . Sending  $\beta \rightarrow +\infty$ , we obtain  $\varphi_{cl}$  and  $\bar{\varphi}_{cl}$  interpolating between the  $Q$ -balls (2.6) at  $\tau \rightarrow -\infty$  and the sector of true vacuum at  $\tau = 0$ . After that the solutions are continued to  $\tau > 0$  using the time reflection symmetry.

Given  $\varphi_{cl}, \bar{\varphi}_{cl}, \eta_0$ , one computes the suppression exponent

$$F_Q = S_E[\varphi_{cl}, \bar{\varphi}_{cl}] - S_E[\varphi_Q, \bar{\varphi}_Q] + \eta_0 Q \quad (2.10)$$

of the decay rate (1.1). Note that the difference of Euclidean actions (2.8) on  $\varphi_{cl}, \bar{\varphi}_{cl}$  and  $Q$ -ball (2.3) in this expression remains finite as  $\beta \rightarrow +\infty$  because our solutions approach  $\varphi_Q, \bar{\varphi}_Q$  at large  $|\tau|$ . The third term in Eq. (2.10) is specific to models with conserved charge  $Q$ . Notably, it involves the parameter  $\eta_0$  from Eq. (2.7) at the place typically occupied by the chemical potential of  $Q$  in statistical physics. In Sec. 3.3 we derive the Legendre transform formula  $dF_Q/dQ = \eta_0$  supporting this intuition.

Our expression for the prefactor in Eq. (1.1) is way more complicated. It uses small perturbations in the background of the semiclassical solution,

$$\varphi = \varphi_{cl} + e^{\omega\tau} \delta\varphi, \quad \bar{\varphi} = \bar{\varphi}_{cl} + e^{-\omega\tau} \delta\bar{\varphi},$$

where  $e^{\pm\omega\tau}$  compensate for exponential behavior of  $\varphi_{cl}$  and  $\bar{\varphi}_{cl}$  as  $\tau \rightarrow \pm\infty$ . The effect of perturbations on the Euclidean action is characterized by its second variation, i.e. the operator

$$\hat{\mathcal{D}}_{cl} = \frac{\delta^2 S_E}{(\delta\varphi, \delta\bar{\varphi})^2} \Big|_{cl} = \begin{pmatrix} V_{cl}'' \bar{\chi}_{cl}^2 & \hat{\mathcal{D}}^- \\ \hat{\mathcal{D}}^+ & V_{cl}'' \chi_{cl}^2 \end{pmatrix}, \quad \hat{\mathcal{D}}^\pm \equiv -(\partial_\tau \pm \omega)^2 - \nabla_{\mathbf{x}}^2 + V_{cl}' + V_{cl}'' \chi_{cl} \bar{\chi}_{cl}. \quad (2.11)$$

Here we introduced the rescaled fields  $\chi_{cl} \equiv e^{-\omega\tau} \varphi_{cl}$  and  $\bar{\chi}_{cl} \equiv e^{\omega\tau} \bar{\varphi}_{cl}$  remaining finite as  $\tau \rightarrow \pm\infty$  and denoted  $V_{cl} \equiv V(\varphi_{cl} \bar{\varphi}_{cl})$ ; the primes are derivatives of this function with respect to its argument. Note that  $\hat{\mathcal{D}}_{cl}$  is Hermitean: it acts on the perturbations  $(\delta\varphi, \delta\bar{\varphi})^T$  vanishing at  $\tau \rightarrow \pm\infty$ . The prefactor in Eq. (1.1) involves determinant of this operator,

$$A_Q = \cosh^2 \eta_0 \left( \frac{B_0}{2\pi} \right)^{1/2} \left[ \frac{-\det' \hat{\mathcal{D}}_{cl}}{\det' \hat{\mathcal{D}}_Q} \right]^{-1/2}, \quad (2.12)$$

where  $\det'$  means that all zero eigenvalues are excluded from the determinant,  $\hat{\mathcal{D}}_Q$  is the same as  $\hat{\mathcal{D}}_{cl}$  but in the  $Q$ -ball background i.e. with  $\chi_{cl}, \bar{\chi}_{cl} \rightarrow \chi_Q(r)$  in Eq. (2.11), the

factors  $\cosh^2 \eta_0$  and  $B_0 = 2 \int d\tau d^3 \mathbf{x} (\partial_\tau \chi_{cl})^2$  were introduced while deleting zero modes from the determinants. Like in the case of bounce, we expect that  $\det' \hat{\mathcal{D}}_{cl}$  has opposite sign to the same determinant  $\det' \hat{\mathcal{D}}_Q$  computed in the background of the metastable solution.

Expression (2.12) for the prefactor seems too involved for practical calculations (see, however, [28, 34, 48, 49]). But it is straightforward to estimate  $A_Q$  by extracting its dependence on the only small parameter in the model — the semiclassical parameter  $g^2 \propto Q_c^{-1}$ . The determinants in Eq. (2.12) do not depend on  $g^2$ , while  $B_0 \propto g^{-2} \sim Q_c$ . One obtains  $A_Q = mQ_c^{1/2}$ , where the mass  $m$  is restored on dimensional grounds.

### 2.3 Applying the method

Now, let us illustrate the semiclassical method in the model (2.1) leaving technical details to Sec. 4. We numerically find the family of semiclassical solutions satisfying Eqs. (2.5), (2.7) and (2.9), then compute their charges by Eq. (2.2). Figure 5 demonstrates profiles  $\rho(r, \tau) \equiv (\varphi_{cl} \bar{\varphi}_{cl})^{1/2}$  of three solutions from this family; the sections  $\tau = \text{const}$  of the solution in Fig. 5b are shown in Fig. 6a. Notably, all our solutions

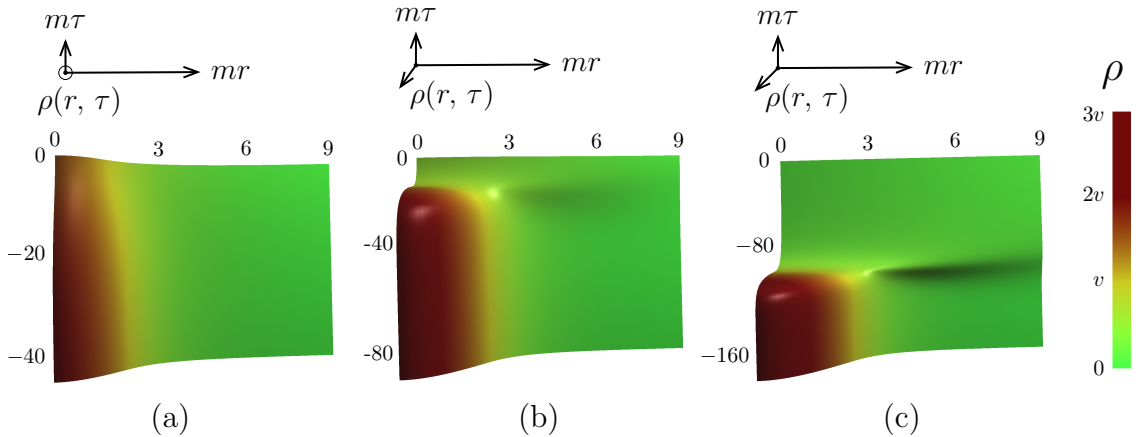


**Figure 5.** Semiclassical solutions  $\rho(r, \tau) \equiv (\varphi_{cl} \bar{\varphi}_{cl})^{1/2}$  describing decay of  $Q$ -balls with  $Q/Q_c \approx 1.05$  (a), 1.33 (b), and 1.56 (c). The parameters of these solutions are marked by open circles in Fig. 4a.

start from the stationary  $Q$ -ball  $\chi_Q(r)$  (points in Fig. 6a) at  $\tau \rightarrow -\infty$  and become lower and wider at  $\tau = 0$  where  $\varphi_{cl} \bar{\varphi}_{cl} < v^2$ . To confirm that they indeed arrive to the vacuum sector, we continue  $\varphi_{cl}$  and  $\bar{\varphi}_{cl}$  to real time by numerically solving the field equations from  $t = \tau = 0$  to large  $t$ , see Fig. 6b. As expected, Minkowski evolution of our solutions describes spreading wave packets corresponding to free particles in the vacuum.

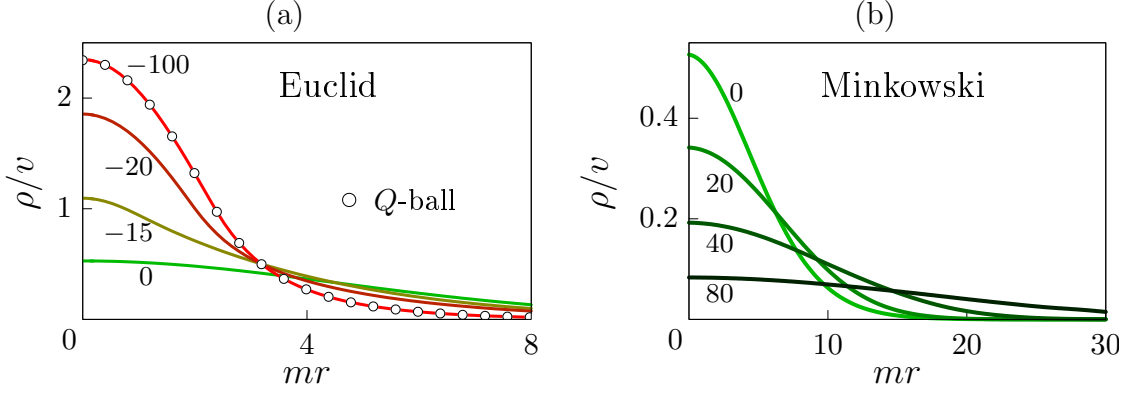


**Figure 6.** (a) Sections  $\tau = \text{const}$  of the semiclassical solution  $\rho(r, \tau) \equiv (\varphi_{cl} \bar{\varphi}_{cl})^{1/2}$  in Fig. 5b (lines). The values of  $m\tau$  are written near the graphs. Empty circles represent the  $Q$ -ball profile  $\chi_Q(r)$  at the same charge. (b) The same semiclassical solution continued to Minkowski time  $t = -i\tau$ . Solid lines show  $\rho(r, t) \equiv |\varphi_{cl}|$  at fixed  $mt$  (numbers near the graphs).

Given the solutions, we numerically compute the suppression exponent (2.10) (solid lines in Figs. 2b and 7a). We see that  $F_Q$  equals zero and infinity at charges  $Q_c$  and  $Q_s$  corresponding to classically unstable and absolutely stable  $Q$ -balls, respectively.

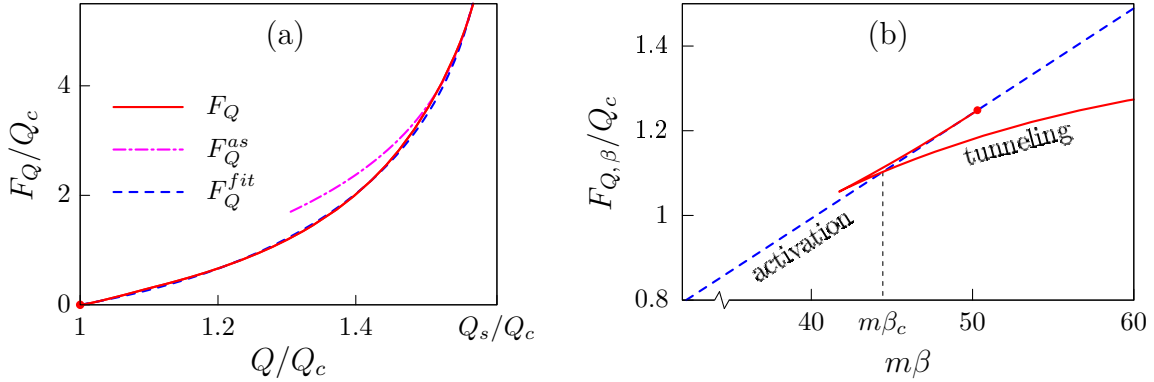


**Figure 7.** (a) Suppression exponent  $F_Q$  for the rate of  $Q$ -ball decay, its  $Q \rightarrow Q_s$  asymptotic  $F_Q^{as}$  and fitting function  $F_Q^{fit}$ , Eqs. (2.13) and (2.14). (b) The exponent  $F_{Q,\beta}$  of thermally induced decay as a function of the inverse temperature  $\beta \equiv T^{-1}$  at  $Q \approx 1.33 Q_c$ . Solid and diagonal-dashed lines are computed using the quasiperiodic Euclidean solutions and  $Q$ -cloud, respectively. The true suppression exponent is given by the least suppressed contribution at each  $\beta$ , i.e. the lowest line on the plot.

To find practical fitting formula for  $F_Q$ , let us study its behavior at  $Q \rightarrow Q_s$  when the total energy deficit  $Q\epsilon_p \equiv E_Q - mQ$  of the decay is small. This corresponds to

small momenta  $p \sim (2m\epsilon_p)^{1/2} \propto (1 - Q/Q_s)^{1/2}$  of the final-state particles/waves and, as a consequence, slow evolution of the solution near  $\tau = 0$ :  $\bar{\varphi}_{cl}\varphi_{cl} \propto e^{\tau\epsilon_p}$ . Thus, large time delay  $\eta_0 \propto \epsilon_p^{-1} \propto (1 - Q/Q_s)^{-1}$  is needed for  $\varphi_{cl}\bar{\varphi}_{cl}$  to approach the  $Q$ -ball profile. Integrating the Legendre formula  $dF_Q/dQ = \eta_0$ , we obtain the asymptotic of the suppression exponent

$$F_Q \rightarrow F_Q^{as} \equiv d_1 + d_2 \log(1 - Q/Q_s) \quad \text{as} \quad Q \rightarrow Q_s. \quad (2.13)$$

Figure 7a demonstrates that Eq. (2.13) (dash-dotted line) is indeed close to  $F_Q$  at  $Q \rightarrow Q_s$  for properly chosen  $d_i$ . Slightly generalizing Eq. (2.13), we obtain the fitting formula in the entire metastability window  $Q_c < Q < Q_s$ ,

$$F_Q \approx F_Q^{fit} = (Q - Q_c) [c_1 + c_2 \log(1 - Q/Q_s)]. \quad (2.14)$$

We find that Eq. (2.14) with  $c_1 = -0.28$  and  $c_2 = -2.6$  describes our numerical results with 5% relative precision, see the dashed line in Fig. 7a.

## 2.4 Decay at finite temperature

Consider metastable  $Q$ -ball immersed into neutral plasma at temperature  $T$ . Thermal fluctuations should decrease the lifetime  $\Gamma_{Q,\beta}^{-1}$  of this object kicking it over the potential barrier in Fig. 4b. Fortunately, our semiclassical method is easily generalized to the case of finite temperature  $T \equiv \beta^{-1}$ : one just considers the above semiclassical solutions in a finite time interval  $-\beta/2 < \tau < \beta/2$  and imposes Eq. (2.7) at  $\tau = -\beta/2$ . This makes the functions  $\varphi_{cl}$  and  $\bar{\varphi}_{cl}$  quasiperiodic: their values at  $\tau = \pm\beta/2$  differ by multiplicative factors  $e^{\pm(\omega\beta + \eta_0)}$ . The suppression exponent is still given by Eq. (2.10), where  $S_E$  is the Euclidean action (2.8) in the interval  $|\tau| < \beta/2$ . Generalization of the prefactor formula (2.12) is slightly less trivial, see comments in Sec. 3.5.

We numerically obtained the quasiperiodic solutions in the model (2.1). Their suppression exponent  $F_{Q,\beta}$  is represented by the solid (“tunneling”) line in Fig. 7b. Notably, the solutions of this kind do not exist at small  $\beta$  and therefore fail to describe thermal transitions in that region. To consider high-temperature processes, we include a trivial semiclassical solution — the  $Q$ -cloud — which has the same form (2.3) as the  $Q$ -ball of the same charge, but with different frequency  $\tilde{\omega}$  and profile  $\tilde{\chi}_Q(r)$ . This solution satisfies Eqs. (2.5), (2.7), (2.9) at arbitrary  $\beta$ . Instead of interpolating between the sectors of  $Q$ -ball and the true vacuum, it simply sits on top of the barrier between them, see Fig. 4b. Computing the exponent (2.10) for the  $Q$ -cloud, one obtains linear function  $F_{Q,\beta} = \beta(\tilde{E}_Q - E_Q)$  shown by the diagonal dashed line in Fig. 7b, where  $\tilde{E}_Q$  is the mass of this object.

The picture in Fig. 7b is typical [50] for thermal transitions, with two semiclassical contributions to the rate representing direct tunneling through the potential barrier

in Fig. 4b and jumps onto its top (activation) induced by thermal fluctuations. The overall suppression exponent corresponds to the least suppressed contribution at each  $\beta$ , given by the “tunneling” and “activation” lines in Fig. 7b at temperatures lower and higher  $\beta_c^{-1}$ , respectively.

As a further generalization of the method, one may consider decay of  $Q$ -ball in charged plasma at temperature  $T$  and chemical potential  $\mu$ . This process, however, is different from the physical viewpoint [51]. The  $Q$ -ball exchanges charge with the medium and reaches equilibrium at  $Q = Q_\mu$ . The respective initial state is described by the grand canonical ensemble giving

$$\Gamma_{\mu,\beta} \propto \int dQ e^{\mu(Q-Q_\mu)-F_{Q,\beta}}$$

for the decay rate, where the prefactors are ignored. This integral is saturated either by one of the integration limits or in the vicinity of the saddle point  $\mu = \eta_0$ ; one has to select the least suppressed contribution at every  $\mu$  and  $\beta$ . We leave this interesting calculation to future studies.

### 3 Derivation of the semiclassical method

We are going to derive the semiclassical expression for the  $Q$ -ball decay rate in two steps. First, we write this rate in the form of path integral. Second, we evaluate the integral in the saddle-point approximation. We will see that this technique is trustworthy at  $Q \gg 1$ .

#### 3.1 Quantum states for $Q$ -balls

The first nontrivial step of our program is to *define* the states of quantum  $Q$ -balls. Note that identification of these objects with the classical solutions (2.3) is not satisfactory in quantum theory where the  $Q$ -ball state  $|Q\rangle$  should be explicitly specified in order to compute its decay amplitude.

Our definition of  $Q$ -balls essentially relies on the presence of a conserved charge in the theory. In the simplest model (1.2) the charge  $Q$  is associated with the phase rotation symmetry  $\varphi \rightarrow e^{-i\alpha}\varphi$ . Then in quantum case the operator  $\hat{Q}$  generates symmetry transformations, i.e. acts as

$$e^{i\alpha\hat{Q}}|\varphi, \bar{\varphi}\rangle = |e^{-i\alpha}\varphi, e^{i\alpha}\bar{\varphi}\rangle \quad (3.1)$$

on the eigenstates  $|\varphi, \bar{\varphi}\rangle$  of field operators  $\hat{\varphi}, \hat{\bar{\varphi}}$  with eigenvalues  $\varphi(\mathbf{x})$  and  $\bar{\varphi}(\mathbf{x})$ . Since  $e^{2\pi i\hat{Q}} = 1$  corresponds to full phase rotation, the charge has integer eigenvalues. Then

the operator

$$\hat{P}_Q = \int_0^{2\pi i} \frac{d\eta}{2\pi i} e^{\eta(\hat{Q}-Q)}, \quad \hat{P}_Q^2 = \hat{P}_Q, \quad (3.2)$$

projects onto the subspace of states with given  $Q$ ; note that integration in Eq. (3.2) is performed along imaginary  $\eta$ .

Using the projector (3.2) one can study the subsector of states with fixed  $Q$ . It is natural to define quantum  $Q$ -ball as a state  $|Q\rangle$  of minimal energy within this subsector [2]. We obtain the limiting formula

$$e^{-\beta\hat{H}/2}\hat{P}_Q|i\rangle \rightarrow e^{-\beta E_Q/2}|Q\rangle\langle Q|i\rangle \quad \text{as} \quad \beta \rightarrow +\infty, \quad (3.3)$$

where  $\hat{P}_Q$  projects an arbitrary state  $|i\rangle$  onto the charge- $Q$  subsector, while the operator  $e^{-\beta\hat{H}/2}$  at large  $\beta$  suppresses all excited states within this subsector leaving only the minimal-energy eigenstate  $|Q\rangle$  of the Hamiltonian  $\hat{H}$ . For simplicity we use normalization<sup>2</sup>  $\langle Q|Q\rangle = 1$ .

In fact, we are interested in small  $Q$ -balls representing local (false) minima of energy at fixed  $Q$ , see Fig. 4b. One can expect that Eq. (3.3) is still applicable in this case if the initial state  $|i\rangle$  belongs to the catchment area of the  $Q$ -ball and Euclidean time interval  $\beta$  is not exponentially large.

### 3.2 Decay probability in the form of path integral

The total probability of  $Q$ -ball decay in time  $t_0$  is obtained by time-evolving the state  $|Q\rangle$  and projecting it onto the basis of Fock states  $|f\rangle$  above the vacuum,

$$\mathcal{P} = \sum_f \left| \langle f | e^{-i\hat{H}t_0} | Q \rangle \right|^2 = e^{\beta E_Q} \sum_{i,f} \left| \langle f | e^{-i\hat{H}(t_0-i\beta/2)} \hat{P}_Q | i \rangle \right|^2, \quad (3.4)$$

where Eq. (3.3) was used to obtain the second equality and the limits  $\beta \rightarrow +\infty$ ,  $t_0 \rightarrow +\infty$  are assumed from now on. Importantly, all initial and final states  $|i\rangle$  and  $|f\rangle$  in Eq. (3.4) belong to the catchment areas of the  $Q$ -ball and true vacuum, respectively. In particular, due to unitarity of quantum evolution one would obtain unit probability,

$$e^{\beta E_Q} \sum_{i,\Psi} \left| \langle \Psi | e^{-i\hat{H}(t_0-i\beta/2)} \hat{P}_Q | i \rangle \right|^2 \rightarrow 1 \quad \text{as} \quad \beta \rightarrow +\infty, \quad (3.5)$$

if summation over all Hilbert states  $|\Psi\rangle$  was performed instead of  $|f\rangle$ .

---

<sup>2</sup>Assuming that a finite spatial box with some boundary conditions is introduced.

To write path integral for the probability (3.4), we use the basis of configuration eigenstates  $|i\rangle \equiv |\varphi_i, \bar{\varphi}_i\rangle$ ,  $|f\rangle \equiv |\varphi_f, \bar{\varphi}_f\rangle$  and Eqs. (3.1), (3.2) for the projector<sup>3</sup>

$$\mathcal{P} = \int_0^{2\pi i} \frac{d\eta}{2\pi i} e^{\beta E_Q - \eta Q} \int \mathcal{D}\varphi_i \mathcal{D}\bar{\varphi}_i \mathcal{D}\varphi_f \mathcal{D}\bar{\varphi}_f \langle \varphi_i, \bar{\varphi}_i | e^{-i\hat{H}(-i\beta/2 - t_0)} | \varphi_f, \bar{\varphi}_f \rangle \\ \times \langle \varphi_f, \bar{\varphi}_f | e^{-i\hat{H}(t_0 - i\beta/2)} | e^{-\eta} \varphi_i, e^{\eta} \bar{\varphi}_i \rangle .$$

One can interpret the propagation operators in this expression as describing time evolution from  $t = i\beta/2$  to  $t = t_0$  to  $t = -i\beta/2$  along the complex time contour  $\mathcal{C}$  in Fig. 8a. Using path integral representation for the evolution operators, one finally arrives at

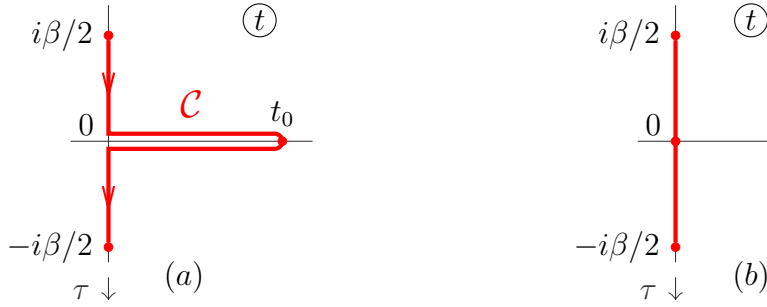


**Figure 8.** (a) Time contour for the path integral (3.6). (b) Equivalent contour.

expression,

$$\mathcal{P} = \int_0^{2\pi i} \frac{d\eta}{2\pi i} e^{\beta E_Q - \eta Q} \int \mathcal{D}\varphi(x) \mathcal{D}\bar{\varphi}(x) e^{iS[\varphi, \bar{\varphi}]}, \quad (3.6)$$

where the configurations  $\varphi(\mathbf{x}, t)$ ,  $\bar{\varphi}(\mathbf{x}, t)$  live on the contour  $\mathcal{C}$  and satisfy quasi-periodic conditions

$$\varphi(\mathbf{x}, t + i\beta) = e^{-\eta} \varphi(\mathbf{x}, t), \quad \bar{\varphi}(\mathbf{x}, t + i\beta) = e^{\eta} \bar{\varphi}(\mathbf{x}, t) \quad (3.7)$$

at  $t = -i\beta/2$ . The classical action  $S[\varphi, \bar{\varphi}]$  is computed along the same contour. Note that the functions  $\varphi$  and  $\bar{\varphi}$  can be continued to the entire Euclidean axis using Eq. (3.7).

Recall that the Euclidean parts of the contour  $\mathcal{C}$  in Fig. 8a are not related to Wick rotation, they appeared due to the minimization procedure (3.3). Thus, representation (3.6) does not rely on analytic properties of the  $Q$ -ball decay amplitude, cf. [29]. Note also that that the “final-state” configurations  $\varphi(\mathbf{x}, t_0) \equiv \varphi_f(\mathbf{x})$  in Eq. (3.6) should

<sup>3</sup>We also exploited the property  $\sum_i \hat{P}_Q |i\rangle \langle i| \hat{P}_Q = \sum_i \hat{P}_Q |i\rangle \langle i|$  which is valid up to exponentially small corrections because the states  $|i\rangle$  belong to the  $Q$ -ball sector, cf. Eq. (3.2).



describe free particles in the vacuum; this makes our integral for the probability essentially different from that for the unity (3.5). Likewise,  $\varphi(\mathbf{x}, \pm i\beta/2)$  should belong to the catchment area of the  $Q$ -ball.

### 3.3 Saddle-point approximation

In Sec. 2.1 we argued that the action  $S$  and charge  $Q$  take large values in the semiclassical regime  $g^2 \ll 1$ . In this case the integral (3.6) of the fast-oscillating exponent  $e^{iS}$  can be evaluated in the saddle-point approximation.

We introduce the saddle-point configuration  $\{\bar{\varphi}_{cl}, \varphi_{cl}, \eta_{cl}\}$  as an extremum of the integrand in Eq. (3.6). It will be convenient to consider  $\varphi_{cl}(\mathbf{x}, \tau)$  and  $\bar{\varphi}_{cl}(\mathbf{x}, \tau)$  as functions of Euclidean time  $\tau \equiv it$  which takes real and imaginary values on the contour in Fig. 8a. By construction,  $\varphi_{cl}$  and  $\bar{\varphi}_{cl}$  satisfy the field equations (2.5) and the boundary conditions (3.7),

$$\varphi_{cl}(\mathbf{x}, \tau + \beta) = e^{\eta_{cl}} \varphi_{cl}(\mathbf{x}, \tau), \quad \bar{\varphi}_{cl}(\mathbf{x}, \tau + \beta) = e^{-\eta_{cl}} \bar{\varphi}_{cl}(\mathbf{x}, \tau). \quad (3.8)$$

Besides, extremization with respect to  $\eta$  gives equation

$$Q = i \frac{dS}{d\eta} = \int d^3 \mathbf{x} [\bar{\varphi}_{cl} \partial_\tau \varphi_{cl} - \varphi_{cl} \partial_\tau \bar{\varphi}_{cl}], \quad (3.9)$$

where Eqs. (2.5), (3.8) were used in the differentiation. Note that Eq. (3.9) coincides with the classical expression (2.2) for the charge. Importantly,  $\varphi_{cl}$  and  $\bar{\varphi}_{cl}$  are not necessarily complex conjugate to each other: integrations in Eq. (3.6) can be continued to independent  $\varphi$ - and  $\bar{\varphi}$ -contours in the functional space.

Solving the field equations (2.5) with the quasiperiodicity conditions (3.8), one obtains the saddle-point configuration  $\{\varphi_{cl}, \bar{\varphi}_{cl}\}$  for every  $\eta_{cl}$ . The latter parameter is then related to the conserved charge by Eq. (3.9).

Now, we compute the integral (3.6) by noting that at  $g^2 \ll 1$  ( $S \gg 1$ ) its integrand is sharply peaked in small vicinity of the saddle point,

$$\varphi = \varphi_{cl} + e^{\omega\tau} \delta\varphi, \quad \bar{\varphi} = \bar{\varphi}_{cl} + e^{-\omega\tau} \delta\bar{\varphi}, \quad \eta = \eta_{cl} + \delta\eta. \quad (3.10)$$

Here the factors  $e^{\pm\omega\tau}$  in front of field perturbations compensate for exponential growth of  $\varphi_{cl}$  and  $\bar{\varphi}_{cl}$  as  $\tau \rightarrow \pm\infty$ , cf. Eq. (2.6). Substituting Eq. (3.10) into Eq. (3.6) and taking the Gaussian integrals over small  $\delta\varphi(\mathbf{x}, \tau)$ ,  $\delta\bar{\varphi}(\mathbf{x}, \tau)$  and  $\delta\eta$ , one obtains the standard saddle-point formula,

$$\mathcal{P} = N \cdot e^{\beta E_Q - \eta_{cl} Q + iS[\varphi_{cl}, \bar{\varphi}_{cl}]} \cdot \frac{\det^{-1/2} \hat{\mathcal{D}}_{cl}}{\sqrt{dQ/d\eta_{cl}}}. \quad (3.11)$$

Here  $N$  is the unknown normalization factor from the functional measure, the second multiplier is the saddle-point value of the integrand, while the determinant of  $\hat{\mathcal{D}}_{cl}$  defined in Eq. (2.11) and the factor  $dQ/d\eta_{cl} = id^2S/d\eta^2$  account for fluctuations of  $\{\delta\varphi, \delta\bar{\varphi}\}$  and  $\delta\eta$ , respectively.

Now, let us simplify the above semiclassical recipe. First, the double-bent Minkowskian part of the contour  $\mathcal{C}$  is redundant: analytic functions  $\varphi_{cl}$  and  $\bar{\varphi}_{cl}$  can be considered on the Euclidean time axis in Fig. 8b. There remains, however, an important selection rule: when continued to real time, these functions should describe the final state with free particles at  $t = t_0 \rightarrow +\infty$ .

Second, the saddle-point equations have two discrete symmetries at  $\tau \in \mathbb{R}$ : simultaneous complex conjugation of all fields  $\varphi_{cl}, \bar{\varphi}_{cl}, \eta_{cl}$  and time reflection

$$\varphi_{cl}(\mathbf{x}, \tau) \rightarrow \bar{\varphi}_{cl}(\mathbf{x}, -\tau), \quad \bar{\varphi}_{cl}(\mathbf{x}, \tau) \rightarrow \varphi_{cl}(\mathbf{x}, -\tau), \quad \eta_{cl} \rightarrow \eta_{cl}.$$

In general case this gives four equally suppressed saddle-point solutions, each producing a term with complex exponent in Eq. (3.11). We expect, however, to find a single dominant saddle-point configuration, just like for other tunneling processes. Then this saddle point is symmetric,

$$\{\varphi_{cl}(\mathbf{x}, \tau), \bar{\varphi}_{cl}(\mathbf{x}, \tau), \eta_{cl}\} \in \mathbb{R}, \quad \varphi_{cl}(\tau, \mathbf{x}) = \bar{\varphi}_{cl}(-\tau, \mathbf{x}) \quad \text{at } \tau \in \mathbb{R}. \quad (3.12)$$

Relations (3.12) turn quasiperiodicity (3.8) into the boundary conditions (2.7), (2.9) at  $\tau = -\beta/2$  and  $\tau = 0$ , where

$$\eta_0 \equiv \eta_{cl} - \omega\beta \quad (3.13)$$

parametrizes the solutions from now on. Notably, Eq. (3.12) implies that  $\varphi_{cl}$  and  $\bar{\varphi}_{cl}$  are complex conjugate to each other on the Minkowski time axis. At real  $t \equiv -i\tau$  they describe classical evolution of waves/particles in the final state. Simultaneously, reality of  $\varphi_{cl}$  and  $\bar{\varphi}_{cl}$  in Euclidean time ensures that the semiclassical expression (3.11) for the probability is real.

Third, let us simplify the leading suppression exponent  $F_Q$  in Eq. (3.11). It is natural to use real Euclidean action  $S_E \equiv -iS$ , Eq. (2.8). The two other terms in the leading exponent can be collected into the action of the stationary  $Q$ -ball, Eq. (2.3),

$$S_E[\varphi_Q, \bar{\varphi}_Q] = \beta E_Q - \omega\beta Q, \quad (3.14)$$

where Eqs. (2.4), (2.8), (3.9) were used. We arrive at the convenient expression (2.10) for  $F_Q$ .

Fourth, it is natural to expect that the semiclassical solution is spherically-symmetric like the  $Q$ -ball, i.e.  $\varphi_{cl}$  and  $\bar{\varphi}_{cl}$  depend on  $r \equiv |\mathbf{x}|$  and  $\tau$ .

Finally, we derive the Legendre transformation formula that was used in Sec. 2. To this end we explicitly differentiate the suppression exponent (2.10) with respect to  $Q$  at fixed  $\beta$ , use Eqs. (3.9), (3.13), (3.14) and the property of  $Q$ -ball  $dE_Q/dQ = \omega$  [1]. We obtain  $dF_Q/dQ = \eta_0$  which gives physical interpretation of  $\eta_0$ . This relation can be also used as a cross-check of numerical calculations.

### 3.4 Expression for the prefactor

Let us further simplify Eq. (3.11). To cancel the unknown constant  $N$ , we divide this expression by unity (3.5) which is given by the same path integral as in Eq. (3.6) but with an important distinction: now the integration runs over all final-state configurations  $\varphi(\mathbf{x}, t_0)$ ,  $\bar{\varphi}(\mathbf{x}, t_0)$ , not just the ones from the vacuum sector. As a consequence, the dominant saddle-point configuration for that integral is the  $Q$ -ball  $\{\varphi_Q, \bar{\varphi}_Q, \eta_0 = 0\}$ , Eq. (2.3). We obtain the saddle-point result similar to Eq. (3.11),

$$1 = N \cdot \frac{\det^{-1/2} \hat{\mathcal{D}}_Q}{\sqrt{dQ/d\eta}}, \quad (3.15)$$

where  $\hat{\mathcal{D}}_Q$  is the same fluctuation operator as in Eq. (3.11) but in the  $Q$ -ball background. Using Eq. (3.13) one finds that  $dQ/d\eta \rightarrow \beta^{-1}dQ/d\omega + O(\beta^{-2})$ . This factor cancels in the ratio of Eqs. (3.11) and (3.15),

$$\mathcal{P} = e^{-F_Q} \cdot \left( \frac{\det \hat{\mathcal{D}}_{cl}}{\det \hat{\mathcal{D}}_Q} \right)^{-1/2}, \quad (3.16)$$

where  $F_Q$  is the suppression exponent from Eq. (3.11).

The operator  $\hat{\mathcal{D}}_{cl}$  introduced in Eq. (2.11) is Hermitean; recall that it acts on perturbations  $\psi \equiv (\delta\varphi, \delta\bar{\varphi})^T$  with quasiperiodic boundary conditions

$$\delta\varphi(\mathbf{x}, \tau + \beta) = e^{\eta_0} \delta\varphi(\mathbf{x}, \tau), \quad \delta\bar{\varphi}(\mathbf{x}, \tau + \beta) = e^{-\eta_0} \delta\bar{\varphi}(\mathbf{x}, \tau), \quad (3.17)$$

cf. Eqs. (3.7) and (3.10). As a consequence, the eigenmodes  $\psi_k(\mathbf{x}, \tau)$  of this operator form orthonormal basis<sup>4</sup> and its eigenvalues  $\lambda_k$  are real,

$$\hat{\mathcal{D}}_{cl}\psi_k = \lambda_k\psi_k, \quad \int_{-\beta/2}^{\beta/2} d\tau d^3\mathbf{x} \psi_k^\dagger \psi_{k'} = \delta_{kk'}, \quad \det \hat{\mathcal{D}}_{cl} = \prod_k \lambda_k. \quad (3.18)$$

We immediately run into a problem:  $\det \hat{\mathcal{D}}_{cl} = 0$  due to zero eigenmodes

$$\psi_0^{(Q)} = B_Q^{-1/2} \begin{pmatrix} \chi_{cl} \\ -\bar{\chi}_{cl} \end{pmatrix}, \quad \psi_0^{(0)} = B_0^{-1/2} \begin{pmatrix} \partial_\tau \chi_{cl} \\ \partial_\tau \bar{\chi}_{cl} \end{pmatrix}, \quad \psi_0^{(i)} = B_i^{-1/2} \begin{pmatrix} \partial_i \chi_{cl} \\ \partial_i \bar{\chi}_{cl} \end{pmatrix}, \quad (3.19)$$

---

<sup>4</sup>We still assume that the finite-size spatial box is introduced.

satisfying  $\hat{\mathcal{D}}_{cl} \psi_0^{(\alpha)} = 0$ , where we introduced fields with finite asymptotics  $\chi_{cl} \equiv e^{-\omega\tau} \varphi_{cl}$ ,  $\bar{\chi}_{cl} \equiv e^{\omega\tau} \bar{\varphi}_{cl}$  and normalization constants  $B_\alpha$ . Indeed, the perturbations (3.19) generate phase rotations  $\varphi \rightarrow e^{-i\alpha} \varphi$ , time and space shifts of the background solution via Eq. (3.10). They do not change the integrand in Eq. (3.6).

It is clear that the functional integration in the directions of zero modes cannot be performed using the saddle-point method. Indeed, in the standard case one represents

$$\begin{pmatrix} \delta\varphi \\ \delta\bar{\varphi} \end{pmatrix} = \sum_k c_k \psi_k(\mathbf{x}, \tau), \quad \mathcal{D}\delta\varphi \mathcal{D}\delta\bar{\varphi} = \prod_k \frac{dc_k}{\sqrt{2\pi}}$$

and takes the Gaussian integrals over  $c_k$ . On the other hand, parameter  $c_0$  in front of  $\psi_0^{(0)}(\mathbf{x}, \tau)$  corresponds to time shift  $\delta t = -ic_0 B_0^{-1/2}$ . The respective integral is not Gaussian; rather, it gives the full period of the process,

$$\int \frac{dc_0}{\sqrt{2\pi}} = it_0 \left( \frac{B_0}{2\pi} \right)^{1/2}. \quad (3.20)$$

Thus, we should exclude zero eigenvalue of  $\psi_0^{(0)}$  from the product in Eq. (3.18) and use Eq. (3.20) instead. Dividing both sides of Eq. (3.16) by  $t_0$ , we obtain expression for the rate  $\Gamma_Q \equiv \mathcal{P}/t_0$ .

The modes due to phase rotations and spatial translations are treated in the same way as  $\psi_0^{(0)}$ . But in contrast to  $\psi_0^{(0)}$ , they exist in the background of  $Q$ -ball; the respective expressions are obtained by changing  $\chi_{cl}, \bar{\chi}_{cl}$  to  $\chi_Q(r)$  in Eq. (3.19). As a consequence, the contributions of these modes partially cancel in Eq. (3.16) leaving the ratios of the normalization constants  $B_\alpha^{1/2}$  computed for the semiclassical solution and  $Q$ -ball, cf. Eq. (3.20). Explicit calculation gives,

$$B_Q \rightarrow \cosh \eta_0 \cdot B_Q|_{\chi_Q}, \quad B_i \rightarrow \cosh \eta_0 \cdot B_i|_{\chi_Q} \quad \text{as } \beta \rightarrow +\infty,$$

where the asymptotics (2.6) were used in Eq. (3.18).

Collecting all factors, we obtain expression (2.12) for the prefactor in Eq. (1.1), where  $\det'$  is the product of all nonzero eigenvalues of the operator and we computed the norm  $B_0$  of  $\psi_0^{(0)}$  using Eq. (3.18). By definition, the determinants in Eq. (2.12) involve quasiperiodic boundary conditions (3.17) with  $\beta \rightarrow +\infty$ . However, once all zero modes are excluded, any kind of boundary conditions with finite  $\delta\varphi$  can be imposed at  $\tau \rightarrow \pm\infty$ . Indeed, the eigenvalue problem for  $\hat{\mathcal{D}}_{cl}$  has the form of a stationary Schrödinger equation for the four-dimensional particle with a spin. The regions  $\tau \rightarrow \pm\infty$  are classically forbidden for this particle: the background solution at large  $|\tau|$  coincides with the  $Q$ -ball which is classically stable, i.e. has only exponentially growing or decaying with  $\tau$  perturbations  $\psi_k$ . It is clear that the values of  $\lambda_k$  do not depend on

the boundary conditions imposed deep inside the classically forbidden regions. Thus, one can consider all determinants in Eq. (2.12) with vanishing boundary conditions  $\delta\varphi, \delta\bar{\varphi} \rightarrow 0$  as  $\tau \rightarrow \pm\infty$  instead of the quasiperiodic ones.

### 3.5 Finite-temperature solutions

Now, consider  $Q$ -ball decay at a finite temperature  $T \equiv \beta^{-1}$ . The initial state of this process is specified by the density matrix  $\hat{\rho}_\beta = Z_\beta e^{-\beta\hat{H}} \hat{P}_Q$ , where  $\hat{P}_Q$  restricts the statistical ensemble to states with charge  $Q$ , while  $Z_\beta$  is a normalization constant ensuring  $\text{tr} \hat{\rho}_\beta = 1$ . As before, we tacitly assume that  $\hat{\rho}_\beta$  is projected onto the states  $|i\rangle$  from the  $Q$ -ball sector. Note, however, that the quantity (3.4) used in the above calculation involves the same density matrix  $\hat{\rho}'_\beta \equiv e^{\beta(E_Q - \hat{H})} \hat{P}_Q$  but with different normalization. Moreover, Eq. (3.5) at finite  $\beta$  gives,

$$e^{\beta E_Q} \sum_{i, \Psi} \left| \langle \Psi | e^{-i\hat{H}(t_0 - i\beta/2)} \hat{P}_Q | i \rangle \right|^2 = \text{tr}_i \rho'_\beta$$

where the trace is taken in the  $Q$ -ball sector. Thus, the ratio of Eqs. (3.4) and (3.5) at finite  $\beta$  that was computed above gives the probability of  $Q$ -ball decay at temperature  $T = \beta^{-1}$ .

We conclude that the exponent  $F_{Q,\beta}$  of thermal decay is given by Eq. (2.10), but with finite time interval  $-\beta/2 < \tau < \beta/2$  in the Euclidean actions (2.8), while the finite- $T$  saddle-point solutions  $\varphi_{cl}, \bar{\varphi}_{cl}$  satisfy Eqs. (2.7) at  $\tau = -\beta/2$ .

To generalize Eq. (2.12) for the prefactor, one should avoid simplifications related to the limit  $\beta \rightarrow +\infty$ . At finite temperature the quantities  $dQ/d\eta_{cl}$  in Eqs. (3.11) and (3.15) do not cancel, the original quasiperiodic conditions (3.17) should be used for all operators, and orthogonal family of zero modes with norms  $B_\alpha$  should be properly defined. We leave derivation of finite-temperature prefactor to interested readers.

## 4 Numerical implementation

In this Section we solve the boundary value problem for the semiclassical solution  $\varphi_{cl}(r, \tau), \bar{\varphi}_{cl}(r, \tau)$ . To this end we adopt units with  $m = 1$  and set  $v = 1$  by field rescaling.

### 4.1 Framework

It is convenient to consider functions with finite asymptotics,

$$y_{cl}(r, \tau) = r e^{-\omega\tau} \varphi_{cl}, \quad \bar{y}_{cl}(r, \tau) = r e^{\omega\tau} \bar{\varphi}_{cl}, \quad (4.1)$$

where  $\omega$  is the frequency of the decaying  $Q$ -ball. We introduce<sup>5</sup>  $N_r \times N_\tau = 150 \times 300$  lattice with sites  $\{r_j, \tau_i\} = \{\Delta r(j+1), -\Delta\tau(i+1/2)\}$ ,  $0 \leq j \leq N_r$ ,  $0 \leq i \leq N_\tau$ , and uniform spacings  $\Delta r$ ,  $\Delta\tau$ . The spatial and temporal extents of our lattice  $r_j < L_r$  and  $-\beta/2 < \tau_i < 0$  are large enough for the solutions to approach their asymptotics:  $L_r = 20$ ,  $\beta = 40 \div 200$ . Our unknowns are the values of  $y_{j,i} \equiv y_{cl}(r_j, \tau_i)$  and  $\bar{y}_{j,i}$  on the lattice sites.

We discretize the field equations (2.5) in the standard second-order manner using

$$\partial_\tau y_{cl}(r_j, \tau_i) \rightarrow \frac{y_{j,i-1} - y_{j,i+1}}{2\Delta\tau}, \quad \partial_\tau^2 y_{cl}(r_j, \tau_i) \rightarrow \frac{y_{j,i-1} + y_{j,i+1} - 2y_{j,i}}{\Delta\tau^2}$$

and similar expressions for the derivatives with respect to  $r$ . Boundary conditions (2.7), (2.9) have natural lattice generalization,

$$\begin{aligned} y_{j,N_\tau} &= \bar{y}_{j,N_\tau-1} e^{-\eta_0} & \bar{y}_{j,N_\tau} &= y_{j,N_\tau-1} e^{\eta_0} \\ y_{j,-1} &= \bar{y}_{j,0}, & \bar{y}_{j,-1} &= y_{j,0}, \end{aligned} \quad (4.2)$$

where  $\tau_0 = -\Delta\tau/2$  and  $\tau_{N_\tau-1} = -\beta/2 + \Delta\tau/2$  are the first and the last lattice sites. Finally, we impose Dirichlet and Neumann conditions at  $r = 0$  and  $L_r$ , respectively,

$$y_{-1,i} = \bar{y}_{-1,i} = 0, \quad y_{N_r,i} = y_{N_r-1,i}, \quad \bar{y}_{N_r,i} = \bar{y}_{N_r-1,i}, \quad (4.3)$$

cf. Eq. (4.1). After discretization Eqs. (2.5) with boundary conditions (4.2), (4.3) constitute a sparse system of  $2N_r N_\tau$  nonlinear algebraic equations for the same number of unknowns  $\varphi_{j,i}$ ,  $\bar{\varphi}_{j,i}$ .

A convenient technique to solve large systems of this kind is provided by the Newton-Raphson method, see e.g. [52]. One starts with the initial guess  $y_{j,i}^{(0)}$ ,  $\bar{y}_{j,i}^{(0)}$  for the solution. Substituting  $y = y^{(0)} + \delta y$ ,  $\bar{y} = \bar{y}^{(0)} + \delta \bar{y}$  into the lattice equations and ignoring nonlinear terms in  $\delta y_{j,i}$ ,  $\delta \bar{y}_{j,i}$ , one arrives at the sparse linear system that gives  $\delta y$  and  $\delta \bar{y}$ . Then one refines the guess by setting  $y^{(0)} \rightarrow y^{(0)} + \delta y$ ,  $\bar{y}^{(0)} \rightarrow \bar{y}^{(0)} + \delta \bar{y}$  and repeats the procedure. The iterations converge to the exact solution if the original guess was good enough. Finally, one adjusts the value of  $\eta_0$  in Eq. (4.2) to fix the charge of the solution to that of the  $Q$ -ball with frequency  $\omega$ . Note that the above algorithm should be supplemented with fast linear solver, cf. [33].

## 4.2 Obtaining the solutions

A drawback of the Newton-Raphson method is its high sensitivity to the initial guess: if  $y^{(0)}$ ,  $\bar{y}^{(0)}$  are not close enough to the semiclassical solution, the method may diverge

---

<sup>5</sup>We take larger  $N_\tau$  for solutions with large periods  $\beta$ .

or produce useless trivial solutions — the  $Q$ -ball,  $Q$ -cloud, or charged condensate in the vacuum. This poses a problem of finding an approximate solution at some  $\beta$  and  $\eta_0$ .

To construct such a solution, we use a nontrivial observation [30] that the (quasi)periodic finite- $\beta$  solutions describe, besides the thermal decays, transitions between the sectors of  $Q$ -ball and vacuum at fixed energies  $E$ . Indeed, thermal density matrix is diagonal in the basis of energy eigenstates, which implies that the semiclassical solutions describing fixed-energy processes contribute with factors  $e^{-\beta E}$  to the thermal rates. This gives physical interpretation to all our quasiperiodic solutions, even the ones producing subleading contributions in Fig. 7b.

A particular semiclassical solution with energy  $E$  close to the  $Q$ -cloud mass  $\tilde{E}_Q$  describes transmission through the infinitesimally small classically forbidden region near the barrier top in Fig. 4b. It should coincide with the  $Q$ -cloud, a configuration “sitting” on top of the barrier, up to small corrections. We demonstrated in Appendix A, however, that almost all small perturbations of the  $Q$ -cloud grow exponentially with  $\tau$  and therefore cannot satisfy the quasiperiodic conditions (2.7). The notable exception is the negative (unstable) mode which periodically depends on  $\tau$  via  $e^{i\gamma\tau}$ . In Fig. 9a we plot the profile  $\xi_-(r)$  of this mode obtained in Appendix A. Adding it to the  $Q$ -cloud

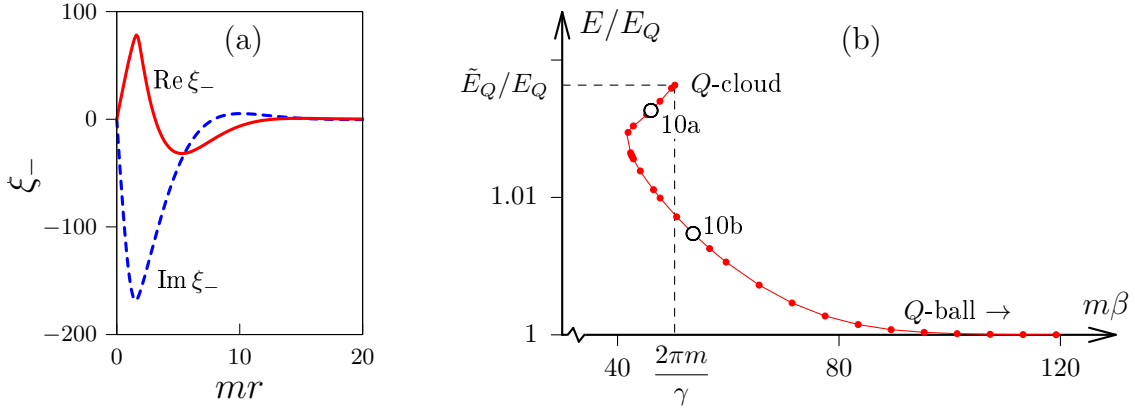


**Figure 9.** (a) Negative mode of the  $Q$ -cloud  $\xi_-(r)$  at  $Q \approx 1.33 Q_c$ . (b) Energies  $E$  of the semiclassical solutions with different Euclidean periods  $\beta$  and the same charge  $Q \approx 1.33 Q_c$  (small filled points). Empty circles with numbers represent solutions in Fig. 10, the solution in Fig. 5b describing  $Q$ -ball decay is obtained in the limit  $\beta \rightarrow +\infty$ .

$\tilde{y}_Q(r)$  we obtain the approximate solution with charge  $Q$  and period  $\beta = 2\pi/\gamma$ ,

$$\begin{aligned} y_{cl} &= [\tilde{y}_Q + A_- (\xi_- e^{-i\gamma\tau} + \xi_-^* e^{i\gamma\tau})] e^{\tau(\tilde{\omega}-\omega)}, \\ \bar{y}_{cl} &= [\tilde{y}_Q + A_- (\xi_- e^{i\gamma\tau} + \xi_-^* e^{-i\gamma\tau})] e^{-\tau(\tilde{\omega}-\omega)}. \end{aligned} \quad (4.4)$$

where we used Eq. (A.2) from Appendix A and recalled that  $\xi_-^*(r) e^{-i\gamma\tau}$  also satisfies the linearized field equations in the background of  $Q$ -cloud. Besides, we introduced the  $Q$ -cloud frequency  $\tilde{\omega}$  and small amplitude  $A_-$  of the perturbation. It is straightforward to check that the configuration (4.4) is real and satisfies the semiclassical equations (2.5), (2.7), (2.9) with  $\eta_0 = \beta(\tilde{\omega} - \omega)$ .

This suggests the following strategy of numerical calculations at a given charge — say, at  $Q \approx 1.33 Q_c$ . We compute the configuration (4.4) with small  $A_- = 10^{-3}$  and use it as an initial guess for the solution with period  $\beta = 2\pi/\gamma - \delta\beta$ ,  $\delta\beta = 0.2$  and  $\eta_0 = 5.7$ . After several Newton-Raphson iterations the new solution is obtained with acceptable precision. Then we use this solution, in turn, as an initial guess at even smaller period  $\beta$ . Continuing to change the value of  $\beta$  in small steps, we obtain a complete<sup>6</sup> branch of solutions shown by points in Fig. 9b, see examples in Fig. 10. At last, we arrive at the solution with large  $\beta$  (Fig. 5b) describing decay of an isolated  $Q$ -ball. The suppression exponents (2.10) of our numerical solutions are shown in Fig. 7b.

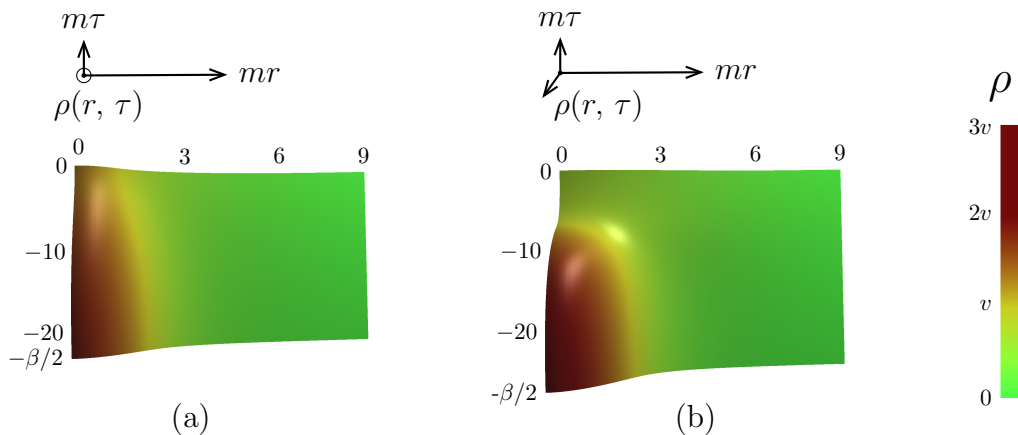


**Figure 10.** Numerical solutions  $\rho = (\varphi\bar{\varphi})^{1/2}$  with  $Q \approx 1.33 Q_c$  and different Euclidean periods: (a)  $m\beta \approx 46$ , (b)  $m\beta \approx 54$ .

Once the solution with large  $\beta$  is found, we start changing  $\omega$  and  $Q(\omega)$  in small steps. As before, at each step we use the solution with charge  $Q$  as an initial guess for the one with charge  $Q \pm \delta Q$ . This gives the semiclassical solutions in the entire

<sup>6</sup>Note that the Newton-Raphson method diverges near the leftmost point of the plot in Fig. 9b where two almost identical solutions with equal periods exist. This restricts the above procedure of small deformations to the upper branch in Fig. 9. Nevertheless, we have found the solutions from the lower branch by using the initial guess (4.4) at  $\beta > 2\pi/\gamma$ , beyond the region of its applicability. We did not need the regular procedure for passing the turn-arounds which prescribes to add Eq. (2.4) to the system of lattice equations and parametrize the solutions with energy  $E$  instead of  $\beta$ .



metastability region  $Q_c < Q < Q_s$ . We compute their suppression exponents (2.10) and obtain Figs. 2b and 7a.

We supported the above numerical procedure with several tests. First, we checked that all numerical solutions with large  $\beta$  are close to the  $Q$ -balls at  $\tau \approx -\beta/2$ , see Fig. 6a, while their energies  $E = E(Q)$  coincide with  $E_Q$ . Second, the suppression exponent  $F_Q$  computed via Eq. (2.10) has the expected properties: it equals zero at  $Q = Q_c$  and grows to infinity as  $Q \rightarrow Q_s$ . Third, the numerical values of  $F_Q$  and  $\eta_0$  are consistent with the Legendre relation  $dF_Q/dQ = \eta_0$ . Fourth, we checked that the semiclassical solutions and the values of  $F_Q$  are not sensitive to the lattice parameters  $L_r, \Delta r, \Delta\tau$  within relative precision of 2%. Besides, we monitored the energy  $E$  and charge  $Q$  of the solutions which were conserved with accuracy better than  $10^{-3}$ . These tests convinced us that the lattice solutions give correct suppression exponent at the precision level of 2%.

## 5 Discussion: Prospects for cosmology

We developed general semiclassical method to calculate the decay rate  $\Gamma_Q = A_Q \cdot e^{-F_Q}$  of metastable  $Q$ -balls at  $Q \gg 1$ . The method can be applied in arbitrary models at the cost of numerically obtaining certain Euclidean solutions  $\varphi_d(\mathbf{x}, \tau)$  that enter the semiclassical expressions for exponent  $F_Q$  and prefactor  $A_Q$  of the rate. We generalized the method to finite-temperature processes.

To illustrate the method, we performed explicit numerical calculations in the model (2.1). In particular, we computed the exponent  $F_Q$  of the  $Q$ -ball decay rate, see Eq. (2.14), and estimated<sup>7</sup> the prefactor  $A_Q \sim mQ_c^{1/2}$ . Notably, the model we use is close to a certain limit of the celebrated Friedberg-Lee-Sirlin (FLS) model [1] which describes complex and real fields  $\varphi$  and  $\zeta$  with renormalizable potential

$$V_{FLS} = (\lambda\zeta^2 - \Lambda^2)^2 + \frac{\Lambda^2}{v^2} \lambda\zeta^2 |\varphi|^2. \quad (5.1)$$

Here  $m \equiv \Lambda^2/v$  and  $m_\zeta \propto \lambda^{1/2}\Lambda$  are masses of the fields,  $\lambda$  is the coupling constant. At  $m_\zeta \gg m$  the field  $\zeta$  is very massive and cannot be excited in processes with relatively low momenta  $p \sim m$ . Minimizing Eq. (5.1) with respect to  $\zeta$  at fixed  $\varphi$ , one obtains low-energy potential for the remaining field,

$$V_{FLS}^{\text{eff}} = \Lambda^4 - \Lambda^4 (1 - |\varphi|^2/2v^2)^2 \theta(2v^2 - |\varphi|^2). \quad (5.2)$$

---

<sup>7</sup>Note that numerical evaluation of the fluctuation determinant in the prefactor involves application of two-dimensional Gelfand-Yaglom theorem and renormalization, which are interesting open tasks beyond the scope of this paper, see [28, 34, 48, 49].

This potential is close to the smooth one, Eq. (2.1) that was used in our calculations, see Fig. 11a. Thus, our numerical data estimate decay rate of the FLS  $Q$ -balls.

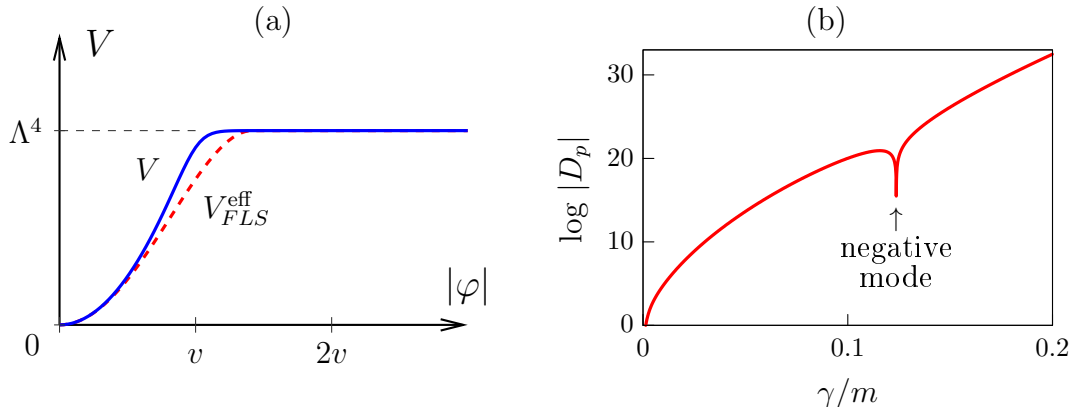


**Figure 11.** (a) Our potential (2.1) compared to the effective low-energy potential (5.2) of the FLS model (solid and dashed lines, respectively). (b) Determinant  $D_p$  of the matrix in Eq. (A.4) as a function of the growth rate  $\gamma$ . The graph is obtained for the  $Q$ -cloud with charge  $Q \approx 1.33 Q_c$ .

Although we did not directly address supersymmetric models with flat directions [21], the decay rate of their  $Q$ -balls is still expected to exhibit the behavior similar to that in Fig. 2b. In particular,  $\Gamma_Q$  should be unsuppressed at the critical charge  $Q_c$  corresponding to classically unstable  $Q$ -ball, it should sharply decrease with charge at  $Q > Q_c$  and reach zero at the point of absolute stability  $Q = Q_s$ . Deep inside the metastability window  $Q_c < Q < Q_s$  the suppression exponent of the rate should be large,  $F_Q \sim Q_c \gg 1$ .

Let us discuss possible cosmological application of metastable  $Q$ -balls with  $Q \sim Q_c$ . These objects may form dark matter with naturally large lifetime, so that their decays in the late-time Universe produce warm dark matter component — energetic  $\varphi$ -particles leaving the galaxies. The latter process may change structure formation or explain [35] appearing tension between the low-redshift [36, 37] and CMB [38] measurements of the Hubble constant.

Note that the decays of dark matter  $Q$ -balls are observable only if their lifetime  $\Gamma_Q^{-1}$  is comparable to the age of the Universe or smaller. This constrains the  $Q$ -ball charge  $Q \sim Q_c \lesssim 150$ , where we used estimates  $F_Q \sim Q_c$ ,  $A_Q \sim m Q_c^{1/2}$  in the mid of the metastability window and assumed wide interval of masses  $m = 1 \text{ eV} \div 10^{19} \text{ GeV}$  in the prefactor. Thus, we need a mechanism to generate small  $Q$ -balls in the early Universe.

The two standard mechanisms of forming dark matter  $Q$ -balls involve phase transition [7–9] or fragmentation of the scalar condensate [10–12] at high temperature  $T$ . Typically, these mechanisms act in a similar way, by collecting charge  $Q$  from the cosmological horizon of size  $H^{-1}$  into the compact objects which further relax into  $Q$ -balls. Assuming initial charge asymmetry<sup>8</sup>  $\Delta_Q = n_Q/s$ , where  $n_Q$  and  $s$  are the charge and entropy densities at temperature  $T$ , one estimates the charges of formed  $Q$ -balls,

$$Q \approx \frac{4\pi}{3} \Delta_Q s H^{-3} \sim \frac{\Delta_Q M_{pl}^3}{T^3 \sqrt{g_*}} \sim 10^2, \quad (5.3)$$

where in the second equality we introduced the number of relativistic degrees of freedom  $g_* \sim 10^2$ , used Friedmann equation  $H \approx g_*^{1/2} T^2 / M_{pl}$  and expression for the entropy density  $s \sim g_* T^3$ . After that we recalled that  $Q \sim 10^2$ . Equation (5.3) relates the generation temperature  $T$  to the asymmetry  $\Delta_Q$ .

The present-day mass density of  $Q$ -balls should coincide with that of dark matter  $\rho_{DM} \sim 10^{-6} \text{ GeV/cm}^3$ . Immediately after generation the concentration of these objects is  $n_{Q\text{-balls}} = n_Q/Q = s\Delta_Q/Q$ . Since expansion of the Universe conserves the ratio  $n_{Q\text{-balls}}/s$ , the mass density of  $Q$ -balls at the present epoch is

$$\frac{E_Q}{Q} s_0 \Delta_Q \approx m s_0 \Delta_Q \sim \rho_{DM}, \quad (5.4)$$

where we introduced the entropy density now  $s_0 \sim 10^3 \text{ cm}^{-3}$  and estimated the mass of a small  $Q$ -balls as  $E_Q \sim mQ$ .

Equations (5.3) and (5.4) relate parameters  $m$ ,  $T$ , and  $\Delta_Q$  of the cosmological model. The standard generation mechanisms naturally work at comparable values of  $m$  and  $T$ . Taking  $T \sim 10^{-2} m$  to prevent immediate decay of  $Q$ -balls due to the temperature fluctuations (see Fig. 7b), we obtain  $\Delta_Q \sim 10^{-22}$  and  $m \sim 10^2 T \sim 10^{13} \text{ GeV}$ . Note that this generation temperature is much higher than the ones in typical models with large  $Q$ -balls, cf. [7–12]. Similar small-mass  $Q$ -balls were considered as natural candidates for self-interacting dark matter [39].

Since the value of  $\Delta_Q$  is way smaller than the observed baryon asymmetry  $\Delta_B \sim 10^{-10}$ , we cannot interpret the charge  $Q$  as the baryon number thus relating small  $Q$ -balls to the Affleck-Dine baryogenesis. Indeed, bold substitution of  $\Delta_Q = \Delta_B$  into Eqs. (5.3), (5.4) gives essentially different values of mass  $m \sim \text{GeV}$  and temperature  $T \sim 10^{15} \text{ GeV}$  which is problematic for the generation mechanisms. Hence, in order to pack the baryon number inside metastable  $Q$ -balls one has to consider special mechanisms of their formation or at least some modification of the standard ones. Alternatively, one can avoid identification of the charge  $Q$  with the baryon number, since cosmology of small metastable  $Q$ -balls is interesting enough by itself.

---

<sup>8</sup>Possibly generated via the Affleck-Dine mechanism [13–15].

**Acknowledgments.** We thank Dmitry Gorbunov and Mikhail Smolyakov for fruitful discussions. This work was supported by the grant RSF 16-12-10494. Numerical calculations were performed on the Computational cluster of the Theory Division of INR RAS.

## A Solitons and their (in)stability

Here we study nontopological solitons in the model (2.1) and linear perturbations in their backgrounds. We use the units with  $m = 1$  and set  $v = 1$  by field rescaling.

We compute the soliton profiles  $\chi_Q(r)$  using the shooting method. First, we substitute the Ansatz (2.3) into the classical field equations and arrive to

$$\partial_r^2 y_Q = -\omega^2 y_Q - V'(y_Q^2/r^2) y_Q, \quad y_Q \equiv r\chi_Q(r) \in \mathbb{R}, \quad (\text{A.1})$$

where the prime is a derivative of  $V$  with respect to its argument. Second, we solve Eq. (A.1) with initial Cauchy data  $y_Q(0) = 0$ ,  $\partial_r y_Q(0) = \chi_0$  at  $r = 0$ . This can be done by many efficient numerical methods. It is convenient, however, to discretize Eq. (A.1) on the same spatial lattice  $\{r_j\}$  as in Sec. 4 and then sequentially determine all  $y_Q(r_j)$  using discrete evolution in Eq. (A.1) from  $r = 0$  to large  $r = r_{N_r}$ . Third, we adjust the parameter  $\chi_0$  in such a way that the Neumann boundary condition  $y_Q(r_{N_r-1}) = y_Q(r_{N_r})$  is satisfied at the rightmost link of the lattice. This gives for every  $\omega$  a real soliton  $\{y_Q(r_j)\}$  which can be conveniently used in the subsequent lattice calculations, see Fig. 3a. The charge  $Q$  and energy  $E_Q$  of the solution are obtained by substituting the Ansatz (2.3) into Eqs. (2.2), (2.4) and computing the integrals over  $r$ .

Now, consider linear instabilities of nontopological solitons. In few models [23, 53] this analysis can be performed analytically, but we need general numerical method to find growing soliton modes. We add small time-dependent perturbation  $\xi_- e^{\gamma t}$  to the soliton profile  $y_Q(r)$ ,

$$\varphi(r, t) = [y_Q(r) + \xi_-(r) e^{\gamma t}] \frac{e^{i\omega t}}{r}, \quad \xi_- = \xi_R + i\xi_I. \quad (\text{A.2})$$

It was shown in [43] that all growing perturbations of this kind, if exist, have real  $\gamma$ . Substituting Eq. (A.2) into the classical field equations and linearizing them with respect to small  $\xi_R$ ,  $\xi_I$ , we find,

$$\begin{aligned} \partial_r^2 \xi_R &= (\gamma^2 - \omega^2) \xi_R - 2\omega\gamma \xi_I + V'_Q \xi_R + 2V''_Q \chi_Q^2 \xi_R, \\ \partial_r^2 \xi_I &= (\gamma^2 - \omega^2) \xi_I + 2\omega\gamma \xi_R + V'_Q \xi_I, \end{aligned} \quad (\text{A.3})$$

where  $V_Q \equiv V(\chi_Q^2)$ . Note that complex conjugate perturbation  $\xi_-^* \equiv \xi_R - i\xi_I$  satisfies Eqs. (A.3) with the growth rate  $(-\gamma)$ .

We want to obtain the parameters  $\gamma$  of regular perturbations  $\xi_R, \xi_I$ . To this end we appeal to the shooting method, again. We discretize Eqs. (A.3) using the lattice  $\{r_j\}$  from Sec. 4 and impose Neumann condition  $\xi_{R,I}(r_{N_r-1}) = \xi_{R,I}(r_{N_r})$  at the rightmost link of the lattice. After that we introduce two basis solutions  $\Psi^{(A)}(r_j) \equiv (\xi_R^{(A)}, \xi_I^{(A)})$  and  $\Psi^{(B)}(r_j)$  satisfying, in addition, the Dirichlet conditions  $\Psi^{(A)}(r_{N_r}) = (1, 0)$  and  $\Psi^{(B)}(r_{N_r}) = (0, 1)$  at the rightmost lattice site. This gives a full set of Cauchy data for  $\Psi^{(A)}(r)$  and  $\Psi^{(B)}(r)$ . Solving Eqs. (A.3) from  $r = r_{N_r}$  to  $r = 0$ , one finds these functions at all lattice sites. Now, recall that we are searching for a specific solution  $\Psi(r_j) = c_A \Psi^{(A)}(r_j) + c_B \Psi^{(B)}(r_j)$  which is regular at the origin, i.e. satisfies  $\Psi(0) = 0$ . This gives the system of linear equations,

$$\hat{D}_p \begin{pmatrix} c_A \\ c_B \end{pmatrix} = 0, \quad \hat{D}_p = \begin{pmatrix} \xi_R^{(A)}(0) & \xi_R^{(B)}(0) \\ \xi_I^{(A)}(0) & \xi_I^{(B)}(0) \end{pmatrix}, \quad (\text{A.4})$$

where the elements of the matrix  $\hat{D}_p$  representing  $\Psi^{(A)}(0)$  and  $\Psi^{(B)}(0)$  are already known. Equation (A.4) has nontrivial solutions only if  $D_p \equiv \det \hat{D}_p = 0$ . In Fig. 11b we plot  $\log |D_p|$  as a function of  $\gamma$  for the  $Q$ -cloud with  $\omega \approx 0.99$ . Parameter  $\gamma$  of the unstable (negative) mode corresponds to a sharp dip in this graph,  $D_p = 0$ . The mode  $\Psi = (\xi_R, \xi_I)$  in Fig. 9a is then obtained using Eq. (A.4) and normalization condition  $c_A^2 + c_B^2 = 1$ .

Performing the above procedure at different  $\omega$ , we learn that all  $Q$ -clouds in Fig. 3b have precisely one unstable mode with  $\gamma > 0$ , while the  $Q$ -balls have none. At the critical point  $dQ/d\omega = 0$  we obtain  $\gamma = 0$ .

## References

- [1] R. Friedberg, T. D. Lee and A. Sirlin, *Class of Scalar-Field Soliton Solutions in Three Space Dimensions*, Phys. Rev. D **13** (1976) 2739.
- [2] S. R. Coleman, *Q-Balls*, Nucl. Phys. B **262** (1985) 263 [*Erratum-ibid*: **269** (1986) 744].
- [3] T. D. Lee and Y. Pang, *Nontopological solitons*, Phys. Rept. **221** (1992) 251.
- [4] A. G. Cohen, S. R. Coleman, H. Georgi and A. Manohar, *The Evaporation of Q-Balls*, Nucl. Phys. B **272** (1986) 301.
- [5] T. Multamaki and I. Vilja, *Analytical and numerical properties of Q-balls*, Nucl. Phys. B **574** (2000) 130 [[hep-ph/9908446](https://arxiv.org/abs/hep-ph/9908446)].
- [6] D. S. Gorbunov and V. A. Rubakov, *Introduction to the theory of the early universe: Hot big bang theory*, World Scientific, 2011.
- [7] J. A. Frieman, G. B. Gelmini, M. Gleiser and E. W. Kolb, *Primordial Origin of Nontopological Solitons*, Phys. Rev. Lett. **60** (1988) 2101.

- [8] K. Griest, E. W. Kolb and A. Massarotti, *Statistical Fluctuations as the Origin of Nontopological Solitons*, Phys. Rev. D **40** (1989) 3529.
- [9] E. Krylov, A. Levin and V. Rubakov, *Cosmological phase transition, baryon asymmetry and dark matter Q-balls*, Phys. Rev. D **87** (2013) 083528 [[arXiv:1301.0354](#)].
- [10] A. Kusenko and M. E. Shaposhnikov, *Supersymmetric Q-balls as dark matter*, Phys. Lett. B **418** (1998) 46 [[hep-ph/9709492](#)].
- [11] S. Kasuya and M. Kawasaki, *Q-ball dark matter and baryogenesis in high-scale inflation*, Phys. Lett. B **739** (2014) 174 [[arXiv:1408.1176](#)].
- [12] S.-Y. Zhou, *Gravitational waves from Affleck-Dine condensate fragmentation*, JCAP **1506** (2015) 033 [[arXiv:1501.01217](#)].
- [13] I. Affleck and M. Dine, *A New Mechanism for Baryogenesis*, Nucl. Phys. B **249** (1985) 361.
- [14] M. Dine and A. Kusenko, *Origin of the matter - antimatter asymmetry*, Rev. Mod. Phys. **76** (2003) 1 [[hep-ph/0303065](#)].
- [15] R. Allahverdi and A. Mazumdar, *A mini review on Affleck-Dine baryogenesis*, New J. Phys. **14** (2012) 125013.
- [16] K. Enqvist and J. McDonald, *Q-balls and baryogenesis in the MSSM*, Phys. Lett. B **425** (1998) 309 [[hep-ph/9711514](#)].
- [17] K. Enqvist and J. McDonald, *B-ball baryogenesis and the baryon to dark matter ratio*, Nucl. Phys. B **538** (1999) 321 [[hep-ph/9803380](#)].
- [18] S. Troitsky, *Supermassive dark-matter Q-balls in galactic centers?*, JCAP **1611** (2016) 027 [[arXiv:1510.07132](#)].
- [19] H. Falcke, F. Melia and E. Agol, *Viewing the shadow of the black hole at the galactic center*, Astrophys. J. **528** (2000) L13 [[astro-ph/9912263](#)].
- [20] N. S. Kardashev *et al.*, *Review of scientific topics for the Millimetron space observatory*, Phys.-Usp. **57** (2014) 1199 [Usp. Fiz. Nauk **184** (2014) 1319] [[arXiv:1502.06071](#)].
- [21] K. Enqvist and A. Mazumdar, *Cosmological consequences of MSSM flat directions*, Phys. Rept. **380** (2003) 99 [[hep-ph/0209244](#)].
- [22] F. Giordano [ATLAS and CMS Collaborations], *SUSY searches at the LHC Run2*, Nuovo Cim. C **40** (2017) 2.
- [23] I. E. Gulamov, E. Ya. Nugaev and M. N. Smolyakov, *Analytic Q-ball solutions and their stability in a piecewise parabolic potential*, Phys. Rev. D **87** (2013) 085043 [[arXiv:1303.1173](#)].
- [24] E. Ya. Nugaev and M. N. Smolyakov, *Particle-like Q-balls*, JHEP **1407** (2014) 009 [[arXiv:1311.3418](#)].

- [25] J. A. Freire and D. P. Arovas, *Collapse of a Bose condensate with attractive interactions*, Phys. Rev. A **59** (1999) 1461 [[cond-mat/9803280](#)].
- [26] I. Yu. Kobzarev, L. B. Okun and M. B. Voloshin, *Bubbles in Metastable Vacuum*, Sov. J. Nucl. Phys. **20** (1975) 644 [Yad. Fiz. **20** (1974) 1229].
- [27] S. R. Coleman, *Fate of the False Vacuum: Semiclassical Theory*, Phys. Rev. D **15** (1977) 2929 [*Erratum-ibid*: **16** (1977) 1248].
- [28] C. G. Callan, Jr. and S. R. Coleman, *Fate of the False Vacuum. II. First Quantum Corrections*, Phys. Rev. D **16** (1977) 1762.
- [29] S. R. Coleman, *The Uses of Instantons*, Subnucl. Ser. **15** (1979) 805.
- [30] S. Yu. Khlebnikov, V. A. Rubakov and P. G. Tinyakov, *Periodic instantons and scattering amplitudes*, Nucl. Phys. B **367** (1991) 334.
- [31] S. V. Demidov and D. G. Levkov, *Soliton-antisoliton pair production in particle collisions*, Phys. Rev. Lett. **107** (2011) 071601 [[arXiv:1103.0013](#)].
- [32] S. Demidov and D. Levkov, *High-energy limit of collision-induced false vacuum decay*, JHEP **1506** (2015) 123 [[arXiv:1503.06339](#)].
- [33] S. V. Demidov and D. G. Levkov, *Semiclassical description of soliton-antisoliton pair production in particle collisions*, JHEP **1511** (2015) 066 [[arXiv:1509.07125](#)].
- [34] A. Andreassen, D. Farhi, W. Frost and M. D. Schwartz, *Precision decay rate calculations in quantum field theory*, Phys. Rev. D **95** (2017) 085011 [[arXiv:1604.06090](#)].
- [35] A. Chudaykin, D. Gorbunov and I. Tkachev, *Dark matter component decaying after recombination: Lensing constraints with Planck data*, Phys. Rev. D **94** (2016) 023528 [[arXiv:1602.08121](#)].
- [36] A. G. Riess *et al.*, *A 3% Solution: Determination of the Hubble Constant with the Hubble Space Telescope and Wide Field Camera 3*, Astrophys. J. **730** (2011) 119 [*Erratum-ibid*: **732** (2011) 129] [[arXiv:1103.2976](#)].
- [37] W. L. Freedman *et al.*, *Carnegie Hubble Program: A Mid-Infrared Calibration of the Hubble Constant*, Astrophys. J. **758** (2012) 24 [[arXiv:1208.3281](#)].
- [38] P. A. R. Ade *et al.* [Planck Collaboration], *Planck 2015 results. XIII. Cosmological parameters*, Astron. Astrophys. **594** (2016) A13 [[arXiv:1502.01589](#)].
- [39] A. Kusenko and P. J. Steinhardt, *Q-ball candidates for self-interacting dark matter*, Phys. Rev. Lett. **87** (2001) 141301 [[astro-ph/0106008](#)].
- [40] A. Kusenko, *Small Q balls*, Phys. Lett. B **404** (1997) 285 [[hep-th/9704073](#)].
- [41] N. G. Vakhitov and A. A. Kolokolov, Radiophys. Quantum. Electron. **16** (1971) 783.

- [42] V. E. Zakharov and E. A. Kuznetsov, *Solitons and collapses: two evolution scenarios of nonlinear wave systems* Phys.-Usp. **55** (2012) 535 [Usp. Fiz. Nauk **182** (2012) 569].
- [43] A. G. Panin and M. N. Smolyakov, *Problem with classical stability of  $U(1)$  gauged  $Q$ -balls*, Phys. Rev. D **95** (2017) 065006 [[arXiv:1612.00737](#)].
- [44] E. Nugaev and A. Shkerin, *Toward the correspondence between  $Q$ -clouds and sphalerons*, Phys. Lett. B **747** (2015) 287 [[arXiv:1501.05903](#)].
- [45] F. R. Klinkhamer and N. S. Manton, *A Saddle-Point Solution in the Weinberg-Salam Theory*, Phys. Rev. D **30** (1984) 2212.
- [46] M. G. Alford,  *$Q$ -Clouds*, Nucl. Phys. B **298** (1988) 323.
- [47] M. I. Tsumagari, E. J. Copeland and P. M. Saffin, *Some stationary properties of a  $Q$ -ball in arbitrary space dimensions*, Phys. Rev. D **78** (2008) 065021 [[arXiv:0805.3233](#)].
- [48] J. Baacke and G. Lavrelashvili, *One loop corrections to the metastable vacuum decay*, Phys. Rev. D **69** (2004) 025009 [[hep-th/0307202](#)].
- [49] G. V. Dunne and H. Min, *Beyond the thin-wall approximation: Precise numerical computation of prefactors in false vacuum decay*, Phys. Rev. D **72** (2005) 125004 [[hep-th/0511156](#)].
- [50] A. N. Kuznetsov and P. G. Tinyakov, *Periodic instanton bifurcations and thermal transition rate*, Phys. Lett. B **406** (1997) 76 [[hep-ph/9704242](#)].
- [51] M. Laine and M. E. Shaposhnikov, *Thermodynamics of nontopological solitons*, Nucl. Phys. B **532** (1998) 376 [[hep-ph/9804237](#)].
- [52] W. H. Press, S. A. Teukolsky, W. T. Vetterling and B. P. Flannery, *Numerical Recipes: The Art of Scientific Computing*, Cambridge University Press, 2007.
- [53] G. C. Marques and I. Ventura, *Resonances Within Nonperturbative Methods in Field Theories*, Phys. Rev. D **14** (1976) 1056.